

High-Order Adaptive Extended Stencil FEM (AES-FEM)

Part I: Convergence and Superconvergence*

Xiangmin Jiao^{†‡}

Rebecca Conley[§]

Tristan J. Delaney^{†¶}

Abstract

Finite elements and finite differences are the most widely used methods for solving boundary value problems, and their high-order variants have respective advantages and disadvantages over complex geometries. In this three-part series of papers, we introduce a new hybrid high-order method, based on our recent work on *Adaptive Extended Stencil FEM*, or *AES-FEM* (*Int. J. Num. Meth. Engrg.*, 2016, DOI:10.1002/nme.5246). This method uses variational forms and test functions similar to those of traditional *finite element methods (FEM)*, but uses basis functions similar to those of *generalized finite difference methods (GFDM)*. In this part, we introduce the framework of *generalized weighted residual methods (GWRM)* to unify FEM, GFDM, and AES-FEM in terms of formulation as well as their accuracy and stability analysis with homogeneous boundary conditions. We also propose a unified treatment under the GWRM framework, and analyze their accuracy and stability over polygonal domains. In Part II and III, we will address the additional challenges associated with general boundary conditions, curved domains, discontinuities, and systems of PDEs.

Keywords: boundary value problems; generalized weighted residuals; finite element methods; high-order accuracy; stability; generalized Lagrange polynomial basis; superconvergence

1 Introduction

Finite elements and finite differences are the most widely used numerical methods for solving elliptic and parabolic partial differential equations (PDEs), or more precisely, as the spatial discretization for their associated boundary value problems (BVPs). The finite element methods (FEM) have been arguably the most successful methods for solving BVPs over complex geometries in engineering applications, because of their flexibilities with unstructured meshes; see, e.g., [17]. The finite difference methods (FDM) have been more thoroughly studied by numerical analysts; see, e.g., [16]. They were traditionally limited to structured meshes, but their generalizations, known as the *generalized finite difference method (GFDM)* [2], have been successfully applied to unstructured meshes and point clouds in recent years.

The focus of this paper is on *high-order* methods over complex geometries, which are of interest both theoretically and practically. By high order, we mean third- or higher-order accuracy in terms of the solution itself, and second- or higher-order accuracy of the gradient of the solutions for applications that require it. Theoretically, high-order methods can deliver better accuracy at lower mesh resolution and can enable the use of lower-precision floating-point arithmetic without having rounding errors dominate truncation errors (see Section 4.2 for detail). These can lead to better efficiency in practice. Both FEM and GFDM can potentially achieve high-order accuracy, for example, by using high-degree polynomial basis functions. However, they have their respective advantages and disadvantages. In particular, the variational forms of FEM lower the

*This work was supported in part by DoD-ARO under contract #W911NF0910306 and also in part under the Scientific Discovery through Advanced Computing (SciDAC) program in the US Department of Energy's Office of Science, Office of Advanced Scientific Computing Research through subcontract #462974 with Los Alamos National Laboratory and under a subcontract with Argonne National Laboratory under Contract DE-AC02-06CH11357. The second author acknowledges the support of the Kenny Fund Fellowship of Saint Peter's University.

[†]Dept. of Applied Math. & Stat. and Institute for Advanced Computational Science, Stony Brook University, Stony Brook, NY 11794, USA.

[‡]Corresponding author. Email: xiangmin.jiao@stonybrook.edu.

[§]Dept. of Math., Saint Peter's University, Jersey City, NJ 07306, USA.

[¶]Current address: Synopsys, Inc., Mountain View, CA 94043, USA.

order of differentiation, which can simplify the computation of second-order differential operators and lower the continuity requirement of the basis functions. However, the piecewise nature of the FEM basis functions leads to a dependence on element shapes, and its traditional treatment of Neumann boundary conditions also suffers from suboptimal convergence rates for curved domains. In contrast, the basis functions of GFDM are polynomials, which are smooth over a small neighborhood of each node and do not depend on element shapes. In addition, it is easy to treat Neumann boundary conditions along curved boundaries at the same accuracy as the interior in GFDM. However, the second-order differential operators must be computed in a brute-force fashion, and there are complications if a Neumann node is at a corner, where the normal is ill-defined.

Traditionally, the analyses of FEM and (G)FDM are typically done using different techniques. Specifically, FEM is typically analyzed based on functional analysis, using the terminologies of Hilbert and Banach spaces. In contrast, FDM is typically analyzed using Fourier and matrix analysis. The main commonality between them is probably just the Taylor series, which are used in their respective (local) consistency analyses. However, even this aspect is different, because the basis functions in FEM are piecewise polynomials that are smooth only within each element, whereas FDM is typically derived using the “method of undetermined coefficients.” To the best of our knowledge, there was not a unified theory that can analyze both classes of methods. This lack of unification made it difficult to develop hybrid high-order methods that combine the advantages of these methods to overcome each other’s disadvantages.

The goal of this three-part series is to develop such a unified framework and a hybrid method for complex geometries based on this framework, for practical applications. Our method is based on an extension of the *adaptive extended stencil finite element method* or *AES-FEM* (pronounced “ace”-F-E-M) [4]. AES-FEM uses the variational forms and test functions similar to those in FEM, and uses the polynomial basis functions similar to those of GFDM. In [4], it was shown that AES-FEM is independent of element shapes and hence simplifies mesh generation. This is analogous to GFDM, and at the same time, AES-FEM enjoys the advantages of FEM in terms of potentially simplifying the computation of second-order differential operators. Furthermore, AES-FEM was shown to achieve second-order convergence with quadratic GLP basis functions, which in general can be constructed with the same local support as piecewise linear FEM. However, a number of issues remained open in [4] in terms of high-order AES-FEM, treatment of Neumann boundary conditions on curved geometries, systems of PDEs, etc.

We address the aforementioned issues in this series of papers. In this part, we introduce the concept of *generalized weighted residual methods* (*GWRM*) to unify FEM, GFDM, and AES-FEM. We then develop a stability analysis of GWRM, which generalizes the well-known *inf-sup condition* for FEM (a.k.a. the Banach-Nečas-Babuška (BNB) theorem) [7] and the Fourier analysis for FDM [16]. Coupled with consistency analysis, this stability analysis allows us to establish the high-order convergence of GFDM and AES-FEM, including superconvergence for meshes with some symmetric structures. We assume homogeneous boundary conditions in this part for simplicity. In Part II, we will introduce a unified treatment of boundary conditions for GWRM, including curved domains and domains with corners, extend our analysis to general boundary conditions, and also present a systematic comparison of several GWRM methods. In Part III, we consider the applications of AES-FEM for systems of PDEs as well as the post-processing for the high-order reconstruction of gradients.

The remainder of this paper is organized as follows. Section 2 reviews the FEM and (G)FDM for boundary value problems, as well as their respective classical analysis. Section 3 introduces the concept of generalized weighted residuals, of which FEM and GFDM are special cases, and AES-FEM is their hybrid in the same framework. Section 4 establishes a unified convergence analysis of GWRM with homogeneous boundary conditions and analyzes the worst-case convergence rates. Section 5 analyzes three sources of superconvergence in GWRM, especially those in GFDM and AES-FEM. Section 6 concludes this paper with a discussion on future work.

2 Background on Finite Elements and Finite Differences

In this section, we review FEM and (G)FDM, which are two important classes of methods for solving boundary value problems. We also give a brief overview of the classical analyses of these methods based on functional analysis and draw some important analogies in matrix theory.

2.1 Boundary Value Problems

Let $\Omega \subset \mathbb{R}^d$ be a bounded, piecewise smooth domain with boundary $\Gamma = \Gamma_D \cup \Gamma_N$, where d is typically 1, 2 or 3, and Γ_D and Γ_N denote the Dirichlet and Neumann boundaries, respectively. Let \mathcal{L} be a second-order linear differential operator. Typically, \mathcal{L} has the form of

$$\mathcal{L}u = -\nabla \cdot (\mu \nabla u) + \nu \cdot \nabla u + \omega^2 u, \quad (1)$$

where $\mu \geq 0$ typically corresponds to a diffusion coefficient, ν is a velocity field, and ω is a wavenumber or frequency. \mathcal{L} can be generalized to vector-valued fields, where μ , ν and ω^2 would be replaced by tensors and may depend on additional unknowns. A *boundary value problem* (BVP) corresponding to \mathcal{L} is to find a sufficiently smooth solution u such that

$$\mathcal{L}u = f \quad \text{on } \Omega. \quad (2)$$

This general form is known as the *convection-diffusion-reaction* equations for vector-valued PDEs. For simplicity, we focus on scalar fields with $\mu > 0$ in Part I and II, and we will consider systems of vector-valued PDEs in Part III. If $\mathcal{L} = -\nabla \cdot (\mu \nabla) + \nu \cdot \nabla$ for a given ν , then its corresponding PDE is the *convection-diffusion equation*. If $\mathcal{L} = -\nabla \cdot (\mu \nabla) + \omega^2$, which is known as the *Sturm-Liouville operator* in 1D, then the resulting PDE is the *Helmholtz equation*. In some of these applications, one is interested in computing not only u but also ∇u , which may correspond to the potential and force fields, respectively.

For the BVP to be well-posed, it may be subject to some *Dirichlet* and/or *Neumann boundary conditions* (BCs),

$$u = u_D \quad \text{on } \Gamma_D, \quad (3)$$

$$\partial_{\mathbf{n}} u = g \quad \text{on } \Gamma_N, \quad (4)$$

where $\partial_{\mathbf{n}}$ denotes the normal derivative, i.e., $\partial_{\mathbf{n}} \equiv \mathbf{n} \cdot \nabla$. The boundary condition is said to be *homogeneous* if $\Gamma_D = \Gamma$ and $u_D = 0$. More generally, we may have *Robin boundary conditions* instead of the Neumann boundary condition, i.e.,

$$c_1 u + c_2 \partial_{\mathbf{n}} u = g_R \quad \text{on } \Gamma_R. \quad (5)$$

A BVP is *coercive* in infinite dimensions if its corresponding eigenvalue problem is positive definite. This is the case for the Poisson or Helmholtz equations, convection-diffusion equations, linear elasticity, etc. Examples of non-coercive problems include advection-reaction equations, Darcy flows, Stokes equations, etc.

For a more unified analysis, we shall interpret the BVP as a system of PDEs

$$\mathcal{L}u = f \quad \text{on } \Omega^\circ, \quad (6)$$

$$u = u_D \quad \text{on } \Gamma_D, \quad (7)$$

$$\partial_{\mathbf{n}} u = g \quad \text{on } \Gamma_N^\circ, \quad (8)$$

where Ω° denotes the interior of Ω , i.e., $\Omega^\circ = \Omega \setminus \Gamma$, and Γ_N° denotes the interior of Γ_N , i.e., $\Gamma_N^\circ = \Gamma_N \setminus \Gamma_D$. We refer to (6), (7) and (8) as second (assuming $\mu > 0$), zeroth, and first order partial differential equations, respectively. Here, Ω° , Γ_D and Γ_N° partition Ω in that they do not intersect each other and $\Omega = \Omega^\circ \cup \Gamma_D \cup \Gamma_N^\circ$. This notion of a system of PDEs is convenient, since we can directly map each equation to a set of algebraic equations later. In addition, if the BVP has Robin boundary conditions, we can simply replace (8) by (5) on Γ_R° .

2.2 Finite Elements and Weighted Residuals

The finite element methods (FEM) are among the most powerful and successful methods for solving BVPs. Mathematically, FEM can be expressed using the framework of *weighted residuals* [8]. Let u_h denote the approximate solution on a given mesh, such as a triangulation of Ω . The *residual* of (2) corresponding to u_h is $\mathcal{L}u_h - f$. Let $\{\psi_i \mid 1 \leq i \leq n\}$ denote the set of *test (or weight) functions*, which span the *test space* Ψ . A *weighted residual method* requires the residual to be orthogonal to Ψ over Ω , or equivalently,

$$\int_{\Omega} \mathcal{L}u_h \psi_i \, d\mathbf{x} = \int_{\Omega} f \psi_i \, d\mathbf{x}, \quad \text{for } i = 1, \dots, n. \quad (9)$$

In FEM, the test functions ψ_i are (weakly) differentiable and have local support. If the ψ_i form a partition of unity, i.e., $\sum_{i=1}^n \psi_i = 1$, then the method is globally conservative in that $\int_{\Omega} \mathcal{L}u_h \, d\mathbf{x} = \int_{\Omega} f \, d\mathbf{x}$.

To discretize the problem fully, let $\{\phi_j \mid 1 \leq j \leq n\}$ denote a set of basis functions, which span the *solution space* Φ . Let Φ denote the vector containing ϕ_j . We find an approximate solution u_h in Φ , i.e.,

$$u \approx u_h = \Phi^T \mathbf{u}_h, \quad (10)$$

where \mathbf{u}_h is the unknown vector. The basis functions are *Lagrange* if $\phi_j(\mathbf{x}_i) = \delta_{ij}$, the Kronecker delta function; i.e., $\phi_j(\mathbf{x}_i) = 1$ if $i = j$ and $\phi_j(\mathbf{x}_i) = 0$ if $i \neq j$. With Lagrange basis functions, if \mathbf{u}_I is the vector composed of $u(\mathbf{x}_j)$, then $\Phi^T \mathbf{u}_I$ is an *interpolation* of u . Furthermore, the unknown vector \mathbf{u}_h in (10) is composed of approximations to nodal values $u(\mathbf{x}_j)$. In FEM, the basis functions are typically Lagrange piecewise polynomial basis functions, although non-polynomial or non-Lagrange basis functions are sometimes used. An FEM is a *Galerkin method* if $\Phi = \Psi$. In this case, Φ (and Ψ) defines a Hilbert space. If $\Phi \neq \Psi$, the FEM is a *Petrov-Galerkin method*, and Φ and Ψ define a Banach space and a reflexive Banach space, respectively.

For elliptic PDEs, an FEM solves (9) by performing integration by parts and then substituting the boundary conditions (3) and (4) into the resulting integral equation. For the general linear operator \mathcal{L} in (1), we obtain a variational form

$$a(u_h, \psi_i) = \langle f, \psi_i \rangle_{\Omega} + \langle \mu \partial_{\mathbf{n}} u_h, \psi_i \rangle_{\Gamma} \quad (11)$$

for each test function ψ_i , where

$$a(u_h, \psi_i) = \int_{\Omega} \nabla \psi_i \cdot (\mu \nabla u_h) + \boldsymbol{\nu} \cdot \nabla u_h \psi_i + \omega^2 u_h \psi_i \, d\mathbf{x}, \quad (12)$$

is the *bilinear form* after integration by parts, $\langle \cdot, \cdot \rangle_{\Omega}$ denotes the inner product over Ω , i.e.,

$$\langle \phi, \psi \rangle_{\Omega} = \int_{\Omega} \phi \psi \, d\mathbf{x}, \quad (13)$$

and $\langle \cdot, \cdot \rangle_{\Gamma}$ denotes the inner product over Γ . Note that a involves only first-order derivatives and it no longer requires differentiating μ . This simplifies the computation if μ is spatially varying and also lowers the differentiability requirements of the basis functions. This is a major advantage of the variational form versus the original strong form (2). The bilinear form a is *bounded* with respect to Φ and Ψ if it satisfies the *generalized Cauchy-Schwarz inequality*, i.e., $\exists C < \infty$ such that $|a(\phi, \psi)| \leq C \|\phi\|_{L^2} \|\psi\|_{L^2}$ for all $\phi \in \Phi$ and $\psi \in \Psi$, where $\|\cdot\|_{L^2}$ is the shorthand of the L^2 -norm over Ω , i.e.,

$$\|\phi\|_{L^2} = \|\phi\|_{L^2, \Omega} = \sqrt{\langle \phi, \phi \rangle_{\Omega}}. \quad (14)$$

For coercive BVPs in infinite dimensions, a defines the *energy norm*, $\|u\|_E = \sqrt{a(u, u)}$.

Let Ψ_{\circ} denote the vector containing the test functions associated with Ω° . The FEM requires each ψ_{\circ} in Ψ_{\circ} to vanish along Γ , i.e., $\psi_{\circ}|_{\Gamma} = 0$. Hence,

$$a(u_h, \psi_{\circ}) \equiv \langle \mathcal{L}u_h, \psi_{\circ} \rangle_{\Omega}, \quad (15)$$

and the variational form (11) simplifies to

$$a(u_h, \psi_{\circ}) = \langle f, \psi_{\circ} \rangle_{\Omega}. \quad (16)$$

Let Φ_{\circ} denote the vector containing the basis functions associated with Ω° . For homogeneous boundary conditions, u and u_h vanish along Γ . If $\boldsymbol{\nu} = \mathbf{0}$, then the bilinear form a is *symmetric* with respect to u_h and ψ_{\circ} , i.e.,

$$a(u_h, \psi_{\circ}) = a(\psi_{\circ}, u_h). \quad (17)$$

This symmetry plays an important role in the classical convergence analysis of FEM.

The variational form for FEM results in an algebraic equation. Under the assumption of homogeneous boundary conditions, $u_h = \Phi_\circ^T \mathbf{u}_{h,\circ}$. Given n_\circ basis functions ϕ_j in Φ_\circ and n_\circ test functions ψ_i in Ψ_\circ , (16) leads to an $n_\circ \times n_\circ$ linear system

$$\mathbf{A}\mathbf{u}_h = \mathbf{b}, \quad (18)$$

where

$$\mathbf{A} = a \left(\Phi_\circ, \Psi_\circ^T \right)^T = [a(\phi_j, \psi_i)], \quad (19)$$

$$\mathbf{b} = \langle f, \Psi_\circ \rangle_\Omega = [\langle f, \psi_i \rangle_\Omega]. \quad (20)$$

Here, i and j denote the row and column indices of \mathbf{A} , respectively. For Galerkin methods for the Helmholtz equation (i.e., $\boldsymbol{\nu} = \mathbf{0}$ in 1), \mathbf{A} is symmetric in that

$$a(\phi_j, \psi_i) = a(\phi_i, \psi_j). \quad (21)$$

In addition, if $\omega \neq 0$ or a Dirichlet boundary condition is imposed, then \mathbf{A} is positive definite. More specifically, for the Poisson equations (i.e., $\mathcal{L} = -\Delta$), the coefficient matrix \mathbf{A} is known as the *stiffness matrix*, typically denoted by \mathbf{K} , and the vector \mathbf{b} is known as the *load vector*. However, \mathbf{A} is asymmetric if the bilinear form in (17) is asymmetric or if $\Phi \neq \Psi$.

Another important matrix is the *mass matrix*

$$\mathbf{M} = \langle \Phi_\circ, \Psi_\circ^T \rangle_\Omega^T = [\langle \phi_j, \psi_i \rangle_\Omega]. \quad (22)$$

This mass matrix is the coefficient matrix of the *projection* problem

$$\langle \Phi_\circ^T \mathbf{f}_P, \Psi_\circ \rangle_\Omega = \langle f, \Psi_\circ \rangle_\Omega, \quad (23)$$

or equivalently, $\mathbf{M}\mathbf{f}_P = \mathbf{b}$. This projection problem can be viewed as a zeroth-order elliptic problem, and it will be an important base case in the error analysis in Section 5. Given \mathbf{M} , we can rewrite (18) as

$$\mathbf{A}\mathbf{u}_h = \mathbf{M}\mathbf{f}_P. \quad (24)$$

After solving (18) or (24), we obtain $u \approx \Phi^T \mathbf{u}_h$. For applications that require the gradient, $\nabla u \approx (\nabla \Phi^T) \mathbf{u}_h$, which is discontinuous at nodes but is typically reconstructed at nodes using projection. For other types of boundary conditions, additional manipulation of the linear system is needed, as we will elaborate in Part II.

2.3 Finite Differences and Their Generalizations

The finite difference methods (FDM) constitute another important class of numerical methods for solving BVPs. The classical FDM is limited to structured meshes, for which the finite difference operators are determined from polynomial interpolations over the stencils of each node. These methods can be generalized to unstructured meshes or point clouds by using least squares polynomial fittings over the stencils to construct the finite difference operators. The resulting methods are known as the *generalized finite difference method (GFDM)* [13, 2].

The FDM is typically considered as an alternative of weighted residual methods. However, we can also express (G)FDM using the concept of weighted residuals, by generalizing it in two senses. First, we do not require the test functions to be (weakly) differentiable. Second, we allow a different set of basis functions with respect to each test function. Under this generalized notion, the test functions in (G)FDM are Dirac delta functions $\{\delta_{\mathbf{x}_i}\}$ at the nodes $\{\mathbf{x}_i\}$. Since the Dirac delta functions are not weakly differentiable, the integration by parts cannot be used computationally (although the Green's identity is still valid in terms of distributional derivatives). For each test function $\psi_i = \delta_{\mathbf{x}_i}$, (G)FDM has a set of polynomial basis functions that define the finite difference operators over the stencil of \mathbf{x}_i . More specifically, for FDM, these basis functions are the Lagrange polynomials over the stencils in 1D; for GFDM, these basis functions are the *generalized Lagrange polynomials*, which we will elaborate in Section 3.2. We will formalize this generalized notion of weighted residuals in Section 3, which will allow us to introduce AES-FEM and develop a unified analysis of FEM, (G)FDM, and AES-FEM.

2.4 Functional Analyses of FEM and FDM

The classical analyses of FEM and FDM are deeply rooted in functional analyses. We briefly review these classical analyses, of which the understanding is critical for us to develop a unified analysis of FEM, (G)FDM, and AES-FEM on unstructured meshes in 2D and 3D.

For FEM, one of the most fundamental results is the *Banach-Nečas-Babuška (BNB) theorem* [7, p. 84-85] regarding the invertibility of the bilinear form (16). Specifically, the theorem states that an FEM discretization with the specific solution space Φ and test space Ψ is *well-posed* (or *invertible*) if and only if

$$\exists \alpha > 0, \quad \inf_{\phi \in \Phi \setminus \{0\}} \sup_{\psi \in \Psi \setminus \{0\}} \frac{a(\phi, \psi)}{\|\phi\|_{\Phi} \|\psi\|_{\Psi}} \geq \alpha \quad (25)$$

and

$$\forall \psi \in \Phi, \quad \sup_{\phi \in \Phi \setminus \{0\}} |a(\phi, \psi)| = 0 \implies \psi = 0, \quad (26)$$

where $\|\cdot\|_{\Phi}$ and $\|\cdot\|_{\Psi}$ are some norms (see below) associated with the spaces Φ and Ψ over Ω , respectively. Eq. (25) is typically referred to the *inf-sup condition*. For coercive problems, which are the focus in this paper, $\|\cdot\|_{\Phi}$ and $\|\cdot\|_{\Psi}$ in (25) typically correspond to the L^2 -norm over Ω as defined in (14). In this case, for Galerkin methods, where $\Phi = \Psi$ is a Hilbert space, the BNB theorem reduces to the *Lax-Milgram theorem* [7, p. 83]. For non-coercive problems, the H^1 (a.k.a. Sobolev) norm is needed for $\|\cdot\|_{\Phi}$, so that a stable solution prevents spurious oscillations. The FEM is *stable* if α in (25) is independent of mesh resolution. Assuming the mesh is *well-shaped* (and more precisely, *quasiuniform*), this inf-sup condition poses constraints on the compatibility between the basis and test functions.

For the convergence of FEM, there have been three classes of analyses. The first, and the most dominant, is based on Hilbert spaces for coercive PDEs. This involves first bounding the error in the energy norm under some smoothness assumptions, which requires Taylor series expansions within each element. Then, the error in the L^2 -norm is shown to be higher order than the energy norm under some regularity assumptions. This second step is more difficult, and it is typically done for the Poisson equation using the *Aubin-Nitsche duality argument*, also known as “*Nitsche’s trick*” [15, p. 166]. Both steps assume symmetric bilinear forms, which does not hold if $\nu \neq 0$ in (1). In addition, it is difficult to incorporate other approximation errors (known as “*variational crimes*” [15], such as those from the interpolation of the source term or the approximation to the geometry) into the duality argument. The second approach is the Fourier analysis for 1D FEM for Poisson equations in the ℓ^2 -norm; see e.g., [9, 15]. The third approach is based on Green’s functions for Poisson equations, which is particularly successful for proving superconvergence in the ∞ -norm; see, e.g., [5, 6]. The first two approaches are global in nature, while the third is local in nature. The latter two approaches have traditionally been limited to 1D or tensor-product meshes, so the first approach has overwhelmingly dominated the FEM literature.

The classical analysis of FDM for BVPs is much simpler than that of FEM. It involves first determining the order of the local truncation errors and then bounding the (absolute) condition number of the linear system; see, e.g. [16]. The former step is referred to as *local consistency analysis*, which typically involves 1D Taylor series about each node. The latter step is referred to as *stability analysis*, typically done using the Fourier analysis on structured grids.

The classical analyses of FEM and FDM cannot be applied to one another: Although the BNB theorem is a general result for FEM, the inf-sup condition (25) cannot be applied to FDM or GFDM, because neither the test functions nor the basis functions in (G)FDM span a Banach space over Ω . Conversely, the Fourier analysis used in FDM is not applicable to FEM on unstructured meshes in 2D and 3D. In terms of GFDM, its consistency analysis is similar to that of FDM by using d -dimensional Taylor series. However, the classical stability analyses of FEM (namely, the inf-sup condition) and of FDM (namely, Fourier analysis) do not apply to GFDM. In the literature, the stability analysis of GFDM has focused on the temporal aspect for parabolic or hyperbolic PDEs; see, e.g., [2]. To the best of our knowledge, there was no general stability analysis of GFDM for BVPs on unstructured meshes.

To develop a unified analysis of FEM, (G)FDM, and AES-FEM, we must distill the most useful concepts in the classical analyses and then generalize them to be independent of tensor-product structure of basis functions, symmetry of bilinear forms, and weak differentiability of test functions. Ideally, the generalizations should enable us to analyze consistency locally whenever possible, instead of mixing consistency and stability

in the same global analysis. The most obvious component for local consistency analysis is the Taylor series. In d -dimensions, it can be written as

$$u(\mathbf{x}_0 + \mathbf{h}) = \sum_{q=0}^p \frac{1}{q!} \nabla^q u(\mathbf{x}_0) \bullet \mathbf{h}^q + \frac{C \|\nabla^{p+1} u(\mathbf{x}_0 + \boldsymbol{\xi})\|}{(p+1)!} \|\mathbf{h}\|^{p+1}, \quad (27)$$

where ∇^q denotes the q th-order derivative tensor, \mathbf{h}^q denote the q th tensor power of \mathbf{h} , “ \bullet ” denotes the scalar product of q th-order tensors, $\|\boldsymbol{\xi}\| \leq \|\mathbf{h}\|$, and $|C| \leq 1$; see, e.g., [10] for a proof. Another useful technique for local analysis is Green’s function, which we will generalize to unstructured meshes in Section 3.3 by using a notion of *discrete Green’s functions*. For stability analysis, we will unify the inf-sup condition and Fourier analysis by introducing a notion of *discrete inf-sup condition* in Section 4.

2.5 Basics of Matrix Analysis

We review some facts in linear algebra, which are critical in unifying, and generalizing, the classical analysis of FEM and FDM.

Given a matrix $\mathbf{A} \in \mathbb{R}^{m \times n}$, its (reduced) singular value decomposition is

$$\mathbf{A} = \mathbf{U} \boldsymbol{\Sigma} \mathbf{V}^T, \quad (28)$$

where $\boldsymbol{\Sigma} = \text{diag}\{\sigma_1, \sigma_2, \dots, \sigma_{\min\{m, n\}}\}$ is composed of the singular values, and \mathbf{u}_i and \mathbf{v}_i for $i = 1, \dots, \min\{m, n\}$ are the left and right singular vectors of \mathbf{A} , respectively. By convention, the singular values are sorted in descending order, i.e., $\sigma_i \geq \sigma_{i+1}$. We will use σ_{\max} and σ_{\min} to denote the largest and smallest singular values of \mathbf{A} , respectively; i.e., $\sigma_{\max} = \sigma_1$ and $\sigma_{\min} = \sigma_{\min\{m, n\}}$. Note that $\sigma_i(\mathbf{A}) = \sigma_i(\mathbf{A}^T)$ for $i = 1, 2, \dots, \min\{m, n\}$. If a matrix $\mathbf{A} \in \mathbb{R}^{n \times n}$ is symmetric and positive definite, then the singular values are the same as the eigenvalues. In this case, we will use λ_i to denote the eigenvalues and use λ_{\max} and λ_{\min} to denote the extreme eigenvalues.

The 2-norm of \mathbf{A} is

$$\|\mathbf{A}\| = \sigma_{\max}(\mathbf{A}) = \sup_{\|\mathbf{v}\|=1} \mathbf{A}\mathbf{v}, \quad (29)$$

which holds regardless of m and n . More generally, the p -norm of \mathbf{A} is $\|\mathbf{A}\|_p = \sup_{\|\mathbf{v}\|_p=1} \|\mathbf{A}\mathbf{v}\|_p$, where $1 \leq p \leq \infty$. If \mathbf{A} has full rank, then the *pseudoinverse* of \mathbf{A} is $\mathbf{A}^+ = \mathbf{V} \boldsymbol{\Sigma}^{-1} \mathbf{U}^T$, which is equal to \mathbf{A}^{-1} if $m = n$. $\|\mathbf{A}^+\| = 1/\sigma_{\min}$. If $m \leq n$, then

$$\|\mathbf{A}^+\|^{-1} = \sigma_{\min}(\mathbf{A}) = \inf_{\|\mathbf{u}\|=1} \mathbf{u}^T \mathbf{A} = \inf_{\mathbf{u} \in \mathbb{R}^m \setminus \{\mathbf{0}\}} \sup_{\mathbf{v} \in \mathbb{R}^n \setminus \{\mathbf{0}\}} \frac{\mathbf{u}^T \mathbf{A} \mathbf{v}}{\|\mathbf{u}\| \|\mathbf{v}\|}. \quad (30)$$

If $m \geq n$, then (30) applies to \mathbf{A}^T instead of \mathbf{A} . The *condition number* of \mathbf{A} in the 2-norm is defined as

$$\kappa(\mathbf{A}) = \|\mathbf{A}\| \|\mathbf{A}^+\| = \frac{\sigma_{\max}(\mathbf{A})}{\sigma_{\min}(\mathbf{A})}. \quad (31)$$

Analogous to the L^2 -norms, the matrix 2-norm satisfies the *Cauchy-Schwarz inequality*, in that $\|\mathbf{AB}\| \leq \|\mathbf{A}\| \|\mathbf{B}\|$. In addition, the inf-sup form in (30) resembles that of the inf-sup condition (25). These connections between functional and matrix analysis will be very useful. They will allow us to restate the BNB theorem for FEM in terms of matrix norms and then generalize it to other methods.

One of the most fundamental techniques in numerical linear algebra is the *backward error analysis*. Assuming a matrix $\mathbf{A} \in \mathbb{R}^{m \times n}$ has full rank, then $\|\mathbf{A}^+\|$ is the *absolute condition number* of the pseudoinverse solution of the linear system

$$\mathbf{Ax} = \mathbf{b} \quad (32)$$

with respect to the perturbation $\delta\mathbf{b}$ in \mathbf{b} . Specifically, let $\tilde{\mathbf{b}} = \mathbf{b} + \delta\mathbf{b}$ and $\tilde{\mathbf{x}} = \mathbf{A}^+ \tilde{\mathbf{b}} = \mathbf{x} + \delta\mathbf{x}$. Then, $\delta\mathbf{x} = \mathbf{A}^+ \delta\mathbf{b}$, and due to the Cauchy-Schwarz inequality,

$$\|\delta\mathbf{x}\| \leq \|\mathbf{A}^+\| \|\delta\tilde{\mathbf{b}}\|, \quad (33)$$

which is tight for some specific \mathbf{b} and $\delta\mathbf{b}$. Note $\kappa(\mathbf{A})$ in (31) is an upper bound of the *relative condition number* of (32) in that

$$\|\delta\mathbf{x}\| / \|\mathbf{x}\| \leq \kappa(\mathbf{A}) \|\delta\tilde{\mathbf{b}}\| / \|\tilde{\mathbf{b}}\|, \quad (34)$$

which is tight for some specific \mathbf{b} and $\delta\mathbf{b}$. The relative condition number is particularly used in analyzing random perturbations (such as rounding errors), but the absolute condition number $\|\mathbf{A}^+\|$ is more useful in analyzing the truncation errors. In this part of the paper, our analysis mostly involves nonsingular matrices, and in this case, we can simply replace the pseudoinverse \mathbf{A}^+ by the inverse \mathbf{A}^{-1} .

3 Generalized Weighted Residuals and AES-FEM

We now introduce the framework of *generalized weighted residuals*, which unifies FEM and (G)FDM. We also introduce AES-FEM as a special case of this framework.

3.1 Generalized Weighted Residuals

As stated in Section 2.3, an important difference between (G)FDM and FEM is that for (G)FDM there is a different set of basis functions at each node. We now generalize the variational forms in Section 2.2 to accommodate (G)FDM.

Let ψ_i denote the test function, i.e., the Dirac delta function, associated with a node \mathbf{x}_i in Ω° . Let Ψ_\circ denote the vector containing these test functions. Let Φ_i denote the vector containing the basis functions associated with ψ_i , where $\phi_{ij} = 0$ if \mathbf{x}_j is not in the stencil of \mathbf{x}_i . The solution of (2) is approximated locally about \mathbf{x}_i by

$$u_{h,i} = \Phi_i^T \mathbf{u}_h.$$

Let the *generalized bilinear form* associated with ψ_i be

$$a(u_{h,i}, \psi_i) = \langle \mathcal{L}u_{h,i}, \psi_i \rangle_\Omega. \quad (35)$$

Note that a in (35) is in general asymmetric, and unlike the bilinear form in FEM, its operators are generalized functions over Ω , including Dirac delta functions, instead of weakly differentiable functions in Banach spaces. Then, we obtain the *generalized variational form* for (G)FDM corresponding to (6) as

$$a(u_{h,i}, \psi_i) = \langle f, \psi_i \rangle_\Omega. \quad (36)$$

Note that (35) and (36) directly generalize (15) and (16) in FEM, respectively, by replacing u_h with $u_{h,i}$. We refer to the formulation as the *generalized weighted residual methods (GWRM)*. Since ψ_i vanishes along Γ , the bilinear form a in (12) remains valid in a distribution sense, although computationally we must use the bilinear form (35).

For BVPs with homogeneous boundary conditions, we can express GWRM in the matrix forms (18) and (24), i.e., $\mathbf{A}\mathbf{u}_h = \mathbf{b}$ or $\mathbf{A}\mathbf{u}_h = \mathbf{M}\mathbf{f}_P$, where

$$\mathbf{A} = \left[a(\Phi_i^T, \psi_i) \right] = [a(\phi_{ij}, \psi_i)], \quad (37)$$

$$\mathbf{b} = [\langle f, \psi_i \rangle_\Omega], \quad (38)$$

$$\mathbf{M} = \left[\langle \Phi_i^T, \psi_i \rangle_\Omega \right] = [\langle \phi_{ij}, \psi_i \rangle_\Omega]. \quad (39)$$

For the Poisson equation, we shall refer to the coefficient matrix as the *stiffness matrix* and refer to \mathbf{b} as the *load vector*. We shall refer to \mathbf{M} as the *mass matrix*, which is the coefficient matrix of the *projection* problem

$$\langle \Phi_i^T \mathbf{f}_P, \psi_i \rangle_\Omega = \langle f, \psi_i \rangle_\Omega, \quad \forall \psi_i \in \Psi_\circ, \quad (40)$$

or equivalently, $\mathbf{M}\mathbf{f}_P = \mathbf{b}$. In particular, for (G)FDM, the i th row in \mathbf{M} is composed of the values of Φ_i , and hence \mathbf{M} is the identity matrix for FDM. For problems that require the gradient, one can approximate it locally as $\nabla u \approx \nabla \Phi_i^T \mathbf{u}_h$. Note that in (37) and (39), we can replace Φ_i with Φ to obtain the stiffness and mass matrices for FEM. Hence, FEM is a special case of GWRM.

3.2 AES-FEM and Generalized Lagrange Polynomials

AES-FEM, or *Adaptive Extended Stencil FEM*, was introduced in [4]. It is convenient to express AES-FEM in the framework of GWRM. The test functions of AES-FEM are similar to those of FEM on Ω° . Specifically, for each node \mathbf{x}_i in Ω° , its corresponding test function is the hat function (a.k.a. pyramid function), which we denoted by $\Lambda_i(\mathbf{x}_i)$. For each test function, AES-FEM has a different set of basis functions, similar to those of GFDM. In this sense, AES-FEM is a hybrid of FEM and GFDM. Since the hat functions are weakly differentiable, just as with FEM, AES-FEM can use integration by parts, which simplifies the computation of the bilinear form especially if μ in (1) is not a constant. In addition, it can enforce Dirichlet boundary conditions strongly. An advantage of AES-FEM, compared to FEM, is that it is independent of element shapes, as shown in [4].

One of the most important aspects of AES-FEM is its basis functions, which we refer to as *generalized Lagrange polynomials (GLP)* basis functions.

Definition 1. Given a set of points $\{\mathbf{x}_j \in \mathbb{R}^d \mid 1 \leq j \leq m\}$, a set of degree- p polynomials $\{\phi_j(\mathbf{x}) \mid 1 \leq j \leq m\}$ constitutes *generalized Lagrange polynomial (GLP) basis functions* corresponding to $\{\mathbf{x}_j\}$ if for every degree- p polynomial $P(\mathbf{x})$, $\sum_{j=1}^m P(\mathbf{x}_j) \phi_j(\mathbf{x})$ fits $P(\mathbf{x})$ exactly.

Let s denote the number of *monomials* up to degree p ; specifically, $s = \prod_{k=1}^d (p+k)/d!$ in d dimensions. In Definition 1, if $m = s$, then the GLP basis functions reduce to the degree- p Lagrange basis functions for polynomial interpolation, which satisfy the property $\phi_j(\mathbf{x}_i) = \delta_{ij}$, the Kronecker delta function. However, in general $m \geq s$ in Definition 1, so these basis functions in general define (weighted) least squares fittings, instead of interpolation, over the points $\{\mathbf{x}_j\}$. Computationally, the Lagrange basis functions for polynomial interpolation are defined by the inverse of the Vandermonde matrix. The GLP basis functions, in contrast, are defined by the pseudoinverse of the Vandermonde matrix; see Appendix A for details. Given m points, the GLP basis functions are not unique, depending on how different points are weighted.

The GLP basis functions can ensure high-order consistency of the polynomial approximations, as stated by the following lemma.

Lemma 2. Given a set of degree- p GLP basis functions $\{\phi_j(\mathbf{x}) \mid 1 \leq j \leq m\}$ over $\{\mathbf{x}_j\}$, if u is continuously differentiable up to p th order, then

$$\left\| \sum_{j=1}^m \nabla^k u(\mathbf{x}_j) \phi_j(\mathbf{x}) - \nabla^k u(\mathbf{x}) \right\|_\infty = \mathcal{O}(h^{p-k+1}), \quad (41)$$

over the neighborhood of $\{\mathbf{x}_j\}$, where h denotes the radius of the neighborhood.

In (41), ∇^k denote the k th derivative, which is a k th order tensor. Note that in [4], the GLP basis functions were defined based on the above property with $k = 0$. Definition 1 above is more constructive, and Lemma 2 is more general.

In the context of AES-FEM, for each node \mathbf{x}_i , we choose a *stencil* of points in its neighborhood, and then construct degree- p GLP basis functions on the stencil. Due to the least-squares nature of GLP basis functions, the number of nodes in the stencil can be chosen adaptively to ensure accuracy and well-conditioning of the Vandermonde system, and hence the name “adaptive extended stencil” in AES-FEM. We will elaborate the adaptive selection of the stencils in Part II.

As an illustration, Figure 1(c) shows a set of five quadratic GLP basis functions associated with a five-node stencil about $\mathbf{x}_i = 0$. As a comparison, we also show the linear and quadratic Lagrange basis functions in 1D over the two elements incident on $\mathbf{x}_i = 0$. Note that there is a key difference between the GLP basis functions in AES-FEM and the Lagrange basis functions in FEM: each FEM basis function is a piecewise polynomial over its local support, whereas each GLP basis function is a true polynomial. Figure 2 illustrates this difference with a 2D FEM hat function and a quadratic GLP basis function. This difference is essential, in that it implies that the bilinear form (15) can be computed in AES-FEM without differentiating a piecewise function defined over an element. This eliminates the dependency of accuracy and stability on element shapes, which is intrinsic to traditional FEM.

AES-FEM, like (G)FDM, does not produce a continuous solution over Ω , due to the local nature of GLP basis functions. This is the key difference between AES-FEM and traditional FEM. We can define a global

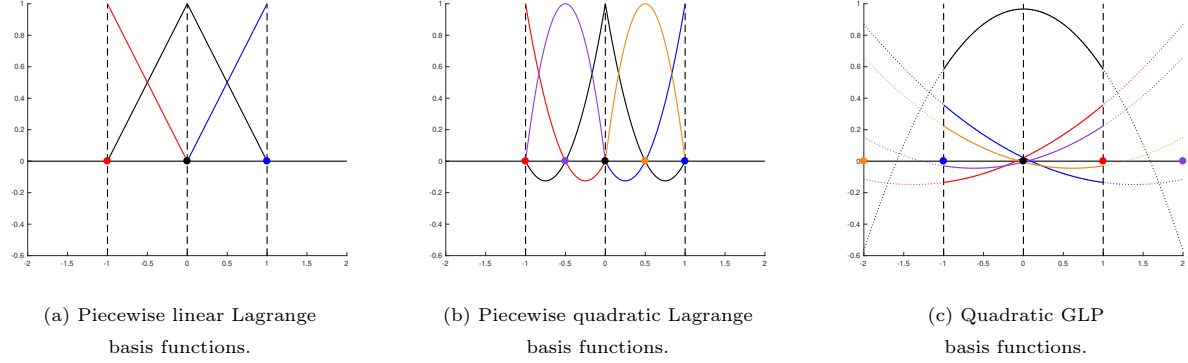


Figure 1: Example basis functions in 1D for linear FEM, quadratic FEM, and quadratic AES-FEM. Each basis function is the same color as the node with which it is associated.

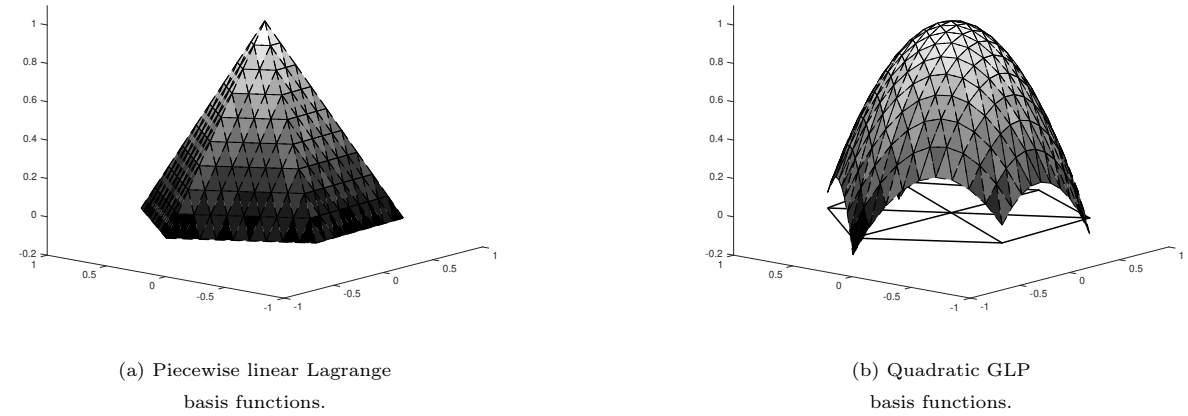


Figure 2: A piecewise basis function in traditional FEM versus a quadratic GLP basis function in AES-FEM. Both basis functions are associated with the center node and have the same stencils.

set of C^0 continuous basis functions by using a weighted averaging of the GLP basis functions, known as *Weighted Averaging of Least Squares* or *WALF* [12]. Using this global set of basis functions in GWRM would result in a Petrov-Galerkin FEM, which we refer to as *continuous AES-FEM*, or *CAES-FEM*. For completeness, Appendix B describes both WALF and CAES-FEM. Like other Petrov-Galerkin FEM, the accuracy of CAES-FEM depends on element shapes, and this dependency defeats the purpose of GLP basis functions. Hence, we will not consider CAES-FEM further but will focus on AES-FEM only.

3.3 Asymmetric Bilinear Form and Discrete Green's Functions

In (17), we say the bilinear form $a(u_h, \psi)$ is *symmetric* if

$$a(u_h, \psi_i) = a(\psi_i, u_h).$$

The symmetry is lost if $\boldsymbol{\nu} \neq \mathbf{0}$ in (1) or if u_h or ψ_i do not vanish along Γ . In GWRM, in general ψ_i vanishes along Γ for an interior node $\mathbf{x}_i \in \Omega^\circ$. However, its local approximate solution $u_{h,i}$, or denoted as u_h for simplicity, may not vanish along Γ if the homogeneous boundary conditions are not enforced explicitly.

For generality, we consider the asymmetric bilinear form associated with the general linear operator \mathcal{L} in (1) at $\mathbf{x}_i \in \Omega^\circ$, i.e.,

$$a(u_h, \psi_i) = \langle \mathcal{L}u_h, \psi_i \rangle_\Omega = \int_\Omega \boldsymbol{\nabla}\psi_i \cdot (\mu \boldsymbol{\nabla}u_h) + \boldsymbol{\nu} \cdot \boldsymbol{\nabla}u_h \psi_i + \omega^2 u_h \psi_i \, d\mathbf{x}.$$

If $\mu = 0$ and $\boldsymbol{\nu} = \mathbf{0}$, then clearly a is symmetric. If $\boldsymbol{\nu} = \mathbf{0}$, $\omega = 0$, and $u_h|_\Gamma = 0$, then a is symmetric because

$$\int_\Omega \boldsymbol{\nabla}\psi_i \cdot (\mu \boldsymbol{\nabla}u_h) \, d\mathbf{x} = - \int_\Omega u_h \boldsymbol{\nabla} \cdot (\mu \boldsymbol{\nabla}\psi_i) \, d\mathbf{x} + \int_\Gamma u_h \mu \partial \mathbf{n} \psi_i \, dS. \quad (42)$$

If $\mu = \omega = 0$, $\boldsymbol{\nu}$ is a constant, and $u_h|_\Gamma = 0$, then a is antisymmetric because

$$\int_\Omega \boldsymbol{\nu} \cdot \boldsymbol{\nabla}u_h \psi_i \, d\mathbf{x} = - \int_\Omega u_h \boldsymbol{\nabla} \cdot (\boldsymbol{\nu} \psi_i) \, d\mathbf{x} + \int_\Gamma u_h \mu \partial \mathbf{n} \psi_i \, dS. \quad (43)$$

The classical analysis of FEM relies on $u_h|_\Gamma = 0$ by assuming homogeneous boundary conditions and $\phi_i|_\Gamma = 0$. For the analysis of asymmetric bilinear forms, we construct a C^2 function \mathcal{G}_i using a notion of *discrete Green's function*, which generalizes the concept of Green's function.

Definition 3. Given a hat function Λ_i corresponding to an interior node $\mathbf{x}_i \in \Omega^\circ$, the *discrete Green's function* of the linear differential operator \mathcal{L} with $\mu > 0$ in (1) associated with ψ_i , denoted by $\mathcal{G}_i(\mathbf{x})$, is the solution to the PDE

$$\mathcal{L}\mathcal{G}_i = \psi_i \quad (44)$$

with homogeneous boundary conditions along Ω_i , where Ω_i is the local support for Λ_i .

If we replace Λ_i with the Dirac delta function $\delta_{\mathbf{x}_i}$ in 1D, then \mathcal{G}_i becomes the classical *Green's function* of \mathcal{L} . This classical definition, however, is not applicable to 2D or 3D. Definition 3 generalizes this classical notion by using the hat function Λ_i as the local source (or impulse) function. Note that Definition 3 requires $\mu > 0$, because (44) is in general ill-posed with homogeneous boundary conditions if $\mu = 0$. It is easy to see that $\|\mathcal{G}_i\|_\infty = \mathcal{O}(h^2)$. In addition, \mathcal{G}_i satisfies the following property.

Lemma 4. *The function value and gradients of the discrete Green's function \mathcal{G}_i of \mathcal{L} in (1) vanish along $\partial\Omega_i$, i.e., $\mathcal{G}_i|_{\partial\Omega_i} = 0$ and $\boldsymbol{\nabla}\mathcal{G}_i|_{\partial\Omega_i} = \mathbf{0}$.*

Proof. Since Λ_i is C^0 over Ω , \mathcal{G}_i is C^2 and $\boldsymbol{\nabla}\mathcal{G}_i$ is C^1 . Since $\mathcal{G}_i = 0$ in $\mathbb{R}^d \setminus \Omega_i$, $\mathcal{G}_i = 0$ along $\partial\Omega_i$. Similarly, since $\boldsymbol{\nabla}\mathcal{G}_i = \mathbf{0}$ in $\mathbb{R}^d \setminus \Omega_i$, $\boldsymbol{\nabla}\mathcal{G}_i = \mathbf{0}$ along $\partial\Omega_i$. \square

If we consider $a(u_h, \mathcal{G}_i)$ instead of $a(u_h, \Lambda_i)$, we can bound the asymmetry as follows.

Theorem 5. For the discrete Green's function \mathcal{G}_i of \mathcal{L} associated with an interior node $\mathbf{x}_i \in \Omega^\circ$

$$\langle \mathcal{L}u_h, \mathcal{G}_i \rangle_\Omega - \langle u_h, \mathcal{L}\mathcal{G}_i \rangle_\Omega = - \int_\Omega u_h (2\boldsymbol{\nu} \cdot \nabla \mathcal{G}_i + \mathcal{G}_i \nabla \cdot \boldsymbol{\nu}) \, d\mathbf{x}. \quad (45)$$

If $\boldsymbol{\nu}$ is a constant, the right-hand side simplifies to $2 \int_\Omega \mathcal{G}_i \boldsymbol{\nu} \cdot \nabla u_h \, d\mathbf{x}$, which vanishes if $\boldsymbol{\nu} = \mathbf{0}$.

Proof. Note that

$$\langle \mathcal{L}u_h, \mathcal{G}_i \rangle_\Omega = \int_\Omega \nabla \mathcal{G}_i \cdot (\mu \nabla u_h) + \mathcal{G}_i \boldsymbol{\nu} \cdot \nabla u_h + \omega^2 u_h \mathcal{G}_i \, d\mathbf{x},$$

and

$$\begin{aligned} \langle u_h, \mathcal{L}\mathcal{G}_i \rangle_\Omega &= \int_\Omega -u_h \nabla \cdot (\mu \nabla \mathcal{G}_i) + u_h \boldsymbol{\nu} \cdot \nabla \mathcal{G}_i + \omega^2 u_h \mathcal{G}_i \, d\mathbf{x} \\ &= \int_\Omega \nabla u_h \cdot (\mu \nabla \mathcal{G}_i) + u_h \boldsymbol{\nu} \cdot \nabla \mathcal{G}_i + \omega^2 u_h \mathcal{G}_i \, d\mathbf{x} - \int_\Gamma u_h (\mu \nabla \mathcal{G}_i \cdot \mathbf{n}) \, dS, \end{aligned}$$

where the second term vanishes due to Lemma 4. Therefore,

$$\langle \mathcal{L}u_h, \mathcal{G}_i \rangle_\Omega - \langle u_h, \mathcal{L}\mathcal{G}_i \rangle_\Omega = \int_\Omega \mathcal{G}_i \boldsymbol{\nu} \cdot \nabla u_h - u_h \boldsymbol{\nu} \cdot \nabla \mathcal{G}_i \, d\mathbf{x}.$$

From Green's identify,

$$\int_\Omega \mathcal{G}_i \boldsymbol{\nu} \cdot \nabla u_h \, d\mathbf{x} = - \int_\Omega u_h \nabla \cdot (\mathcal{G}_i \boldsymbol{\nu}) \, d\mathbf{x} + \int_\Gamma u_h (\boldsymbol{\nu} \cdot \mathcal{G}_i \cdot \mathbf{n}) \, dS,$$

where the second term vanishes due to Lemma 4. Furthermore, $\nabla \cdot (\mathcal{G}_i \boldsymbol{\nu}) = \mathcal{G}_i (\nabla \cdot \boldsymbol{\nu}) + \boldsymbol{\nu} \cdot \nabla \mathcal{G}_i$. Hence,

$$\begin{aligned} \langle \mathcal{L}u_h, \mathcal{G}_i \rangle_\Omega - \langle u_h, \mathcal{L}\mathcal{G}_i \rangle_\Omega &= - \int_\Omega u_h (\nabla \cdot (\mathcal{G}_i \boldsymbol{\nu}) + \boldsymbol{\nu} \cdot \nabla \mathcal{G}_i) \, d\mathbf{x} \\ &= - \int_\Omega u_h (2\boldsymbol{\nu} \cdot \nabla \mathcal{G}_i + \mathcal{G}_i \nabla \cdot \boldsymbol{\nu}) \, d\mathbf{x}. \end{aligned}$$

If $\boldsymbol{\nu}$ is a constant, the second term vanishes; if $\boldsymbol{\nu} = \mathbf{0}$, both terms vanish. \square

Theorem 5 is most relevant to AES-FEM and linear FEM. We will use it in Section 5.1 to analyze the superconvergence of AES-FEM.

4 Convergence of GWRM

We present a unified convergence analysis of GWRM, based on backward error analysis. Our analysis combines the functional and matrix analyses by exploiting their connections as described in Section 2.5.

4.1 Backward Error Analysis of GWRM

Let $\mathbf{u}_h \in \mathbb{R}^n$ denote the unknown solution vector of a GWRM on a mesh with n nodes. Let \mathbf{u}_I denote the vector composed of $u(\mathbf{x}_i)$. We define the *error vector* to be

$$\delta \mathbf{u} = \mathbf{u}_h - \mathbf{u}_I, \quad (46)$$

and define the *residual vector* to be

$$\mathbf{r} = \mathbf{b} - \mathbf{A}\mathbf{u}_I = \mathbf{A}(\mathbf{u}_h - \mathbf{u}_I) = \mathbf{A}\delta \mathbf{u}. \quad (47)$$

Suppose $\mathbf{A} \in \mathbb{R}^{n \times n}$ is nonsingular, and the rounding errors in \mathbf{A} are negligible. Then,

$$\|\delta \mathbf{u}\|_p \leq \|\mathbf{A}^{-1}\|_p \|\mathbf{r}\|_p \quad (48)$$

for any p -norm for $1 \leq p \leq \infty$. The *convergence rate in the p -norm* for the nodal solutions \mathbf{u} is the order of $n^{-\frac{1}{p}} \|\delta\mathbf{u}\|_p$ in terms of mesh resolution.

To establish a connection with functional analysis, let $u_{I,i} = \Phi_i^T \mathbf{u}_I$ and let

$$\delta u_i = u - u_{I,i}. \quad (49)$$

Let $f_{P,i} = \Phi_i^T \mathbf{f}_P$, where $\mathbf{f}_P = \mathbf{M}^{-1} \mathbf{b}$ is the solution of projection (40). Then, the i th entry of \mathbf{r} is

$$\begin{aligned} r_i &= \langle f_{P,i}, \psi_i \rangle_{\Omega} - a(u_{I,i}, \psi_i) \\ &= \langle f_{P,i} - f, \psi_i \rangle_{\Omega} - a(u_{I,i} - u, \psi_i) \quad \{ \text{since } a(u, \psi_i) = \langle f, \psi_i \rangle \} \\ &= a(\delta u_i, \psi_i). \quad \{ \text{since } \langle f_{P,i} - f, \psi_i \rangle = 0 \} \end{aligned}$$

Hence, we obtain the following sufficient condition of the convergence of GWRM.

Lemma 6. *The convergence rate of a GWRM for a boundary value problem is at least q th order in the p -norm if*

$$\max \{|a(\delta u_i, \psi_i)|\} = \|\mathbf{A}^{-1}\|_p^{-1} \mathcal{O}(h^q), \quad (50)$$

where h is the characteristic edge length of the mesh.

Proof. (48) implies

$$n^{-\frac{1}{p}} \|[a(\delta u_i, \psi_i)]\|_p = \|\mathbf{A}^{-1}\|_p^{-1} \mathcal{O}(h^q). \quad (51)$$

Since $n^{-\frac{1}{p}} \|\mathbf{r}\|_p \leq \|\mathbf{r}\|_{\infty}$, (50) follows from (51). \square

More specifically, a GWRM *converges* if $q > 0$ in Lemma 6. However, we are interested in methods with at least second-order accuracy. To use Lemma 6, we need to bound $\|\mathbf{A}^{-1}\|_p$ through *stability analysis*, which is global in nature. We also need to bound $a(\delta u_i, \psi_i)$ using *local consistency analysis*; the ∞ -norm in (50) signifies its local nature. This is similar to the classical analysis of FDM for BVPs, which involves first proving the pointwise convergence of the finite difference operator for \mathcal{L} , followed by proving $\|\mathbf{A}^{-1}\|_p \geq C > 0$ for $p = 2$ or ∞ . Lemma 6 generalizes this process. For simplicity, we will focus on the 2-norm (i.e., $p = 2$ in (50)), also known as the ℓ^2 -norm. This is different from the classical analysis of FEM, which bounds the error in the L^2 , instead of the ℓ^2 , norm. In the following, we define realistic conditions to bound $\|\mathbf{A}^{-1}\|$ and then further derive a more user-friendly version of Lemma 6.

4.2 Stability of GWRM

We first consider the well-posedness of GWRM, by restating the inf-sup condition (25) for FEM using matrix notation.

Definition 7. For GWRM, the *discrete inf-sup condition* is

$$\exists C > 0, \quad \|\mathbf{M}\| \|\mathbf{A}^{-1}\| \leq C, \quad (52)$$

where \mathbf{A} and \mathbf{M} were defined in (37) and (39), respectively.

It is clear that (52) is the necessary and sufficient condition for the *well-posedness* (or *invertibility*) of

$$\mathbf{M}^{-1} \mathbf{A} \mathbf{u}_h = \mathbf{f}_P, \quad (53)$$

which is the rescaled version of (18) and (24), where $\mathbf{f}_P = \mathbf{M}^{-1} \mathbf{b}$. More importantly, Eq. (52) is equivalent to the inf-sup condition (25) for FEM for linear coercive BVPs with *quasiuniform meshes*, as we show in Appendix C. Like FEM, we define a similar concept of *quasiuniformity* for GWRM.

Definition 8. A type of meshes, along with its associated test functions $\{\psi_i\}$ and corresponding basis functions $\{\Phi_i\}$, is *quasiuniform* if

$$\kappa(\mathbf{M}) = \|\mathbf{M}\| \|\mathbf{M}^{-1}\| = \Theta(1) \quad (54)$$

independently of mesh resolution, where \mathbf{M} is the mass matrix as defined in (39). We refer to (54) as the *quasiuniformity condition*.

In (54), $\Theta(1)$ indicates a constant independent of h , and it is equivalent to $\mathcal{O}(1)$ because $\kappa(\mathbf{M}) \geq 1$. Definition 8 refers to a *type* of meshes instead of a single mesh, because the asymptotic bound is with respect to h under mesh refinement. From the discussions in Appendix C, it is clear that the conventional assumption of quasiuniform meshes in FEM implies (54). For FDM, $\mathbf{M} = \mathbf{I}$, and hence (54) is satisfied, and the discrete inf-sup condition (52) reduces to the boundedness of $\|\mathbf{A}^{-1}\|$, which is traditionally shown using Fourier analysis on uniform structured grids.

For GFDM and AES-FEM, the quasiuniformity and discrete inf-sup conditions pose constraints on the local stencils, as well as the compatibility between the test and basis functions. From a practical point of view, quasiuniformity requires that the ratio between the largest and smallest local supports of the test functions is bounded. In addition, the basis functions must be *compatible* with their corresponding test functions with respect to the inner product in (39), so that the inner product does not vanish (e.g., due to cancellation in the integral) and does not blow up (e.g., due to some potential instabilities of the basis functions). Note that quasiuniformity does not exclude adaptive mesh refinement (AMR), though AMR would require a generalization of the definitions, which is beyond the scope of this paper. In addition, we note the following fact.

Theorem 9. *Under the quasiuniformity condition (54), the discrete inf-sup condition (52) is equivalent to*

$$\|\mathbf{A}^{-1}\mathbf{M}\| = \Theta(1), \quad (55)$$

independently of mesh resolution.

Proof. (52) implies (55) because $\|\mathbf{A}^{-1}\mathbf{M}\| \leq \|\mathbf{M}\| \|\mathbf{A}^{-1}\|$. Conversely, (55) implies (52) because $\|\mathbf{M}\| \|\mathbf{A}^{-1}\| = \|\mathbf{M}\| \|\mathbf{A}^{-1}\mathbf{M}\mathbf{M}^{-1}\| \leq \kappa(\mathbf{M}) \|\mathbf{A}^{-1}\mathbf{M}\| = \Theta(1)$. \square

Hence, we can use (52) and (55) interchangeably under the quasiuniformity condition for GWRM with homogeneous boundary conditions.

The classical stability analyses of FDM and FEM require the constants in (52) or (55) to be independent of mesh resolution. It is straightforward to generalize this notion to GWRM.

Definition 10. A GWRM with homogeneous boundary conditions is *stable* if

$$\|\mathbf{A}^{-1}\mathbf{M}\| \leq \|\mathbf{M}\| \|\mathbf{A}^{-1}\| = \Theta(1), \quad (56)$$

independently of mesh resolution. We refer to (56) as the *stability condition*.

Under the quasiuniformity condition, one could use either $\|\mathbf{M}\| \|\mathbf{A}^{-1}\| = \Theta(1)$ or $\|\mathbf{A}^{-1}\mathbf{M}\| = \Theta(1)$ as the stability condition. The former directly corresponds to the classical analysis based on the inf-sup condition in FEM. In the latter, $\|\mathbf{A}^{-1}\mathbf{M}\|$ corresponds to the absolute condition number of the rescaled linear system (53), and it is easier to generalize to more complicated variational forms in Parts II and III. Note that the quasiuniformity condition (54) is equivalent to $\|\mathbf{M}\| \|\mathbf{A}^{-1}\| = \Theta(1)$ with $\mathbf{A} = \mathbf{M}$; in other words, quasiuniformity is the stability of the projection problem (23). In general, the stability condition (56) is reasonable only on quasiuniform meshes.

With the above definitions, we restate Lemma 6 in a more friendly form.

Theorem 11. *Under the stability condition (56), a GWRM for the BVP (2) with homogeneous boundary conditions converges at the rate of at least q th order in the 2-norm if*

$$\max \{|a(\delta u_i, \psi_i)|\} = \|\mathbf{M}\| \mathcal{O}(h^q), \quad (57)$$

where h is the characteristic edge length of the mesh.

Proof. (56) implies $\|\mathbf{A}^{-1}\|^{-1} = \Theta(1) \|\mathbf{M}\|$. Substituting it into (50) and letting $p = 2$, we then obtain (57). \square

From a practical point of view, the stability condition for a general BVP requires that the BVP must be well-posed in infinite dimensions, which determine the constants in (56) and (54) for sufficiently fine meshes.

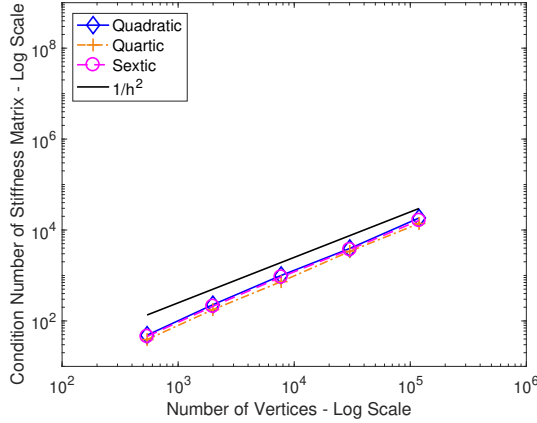


Figure 3: Condition numbers of stiffness matrices of AES-FEM under mesh refinement.

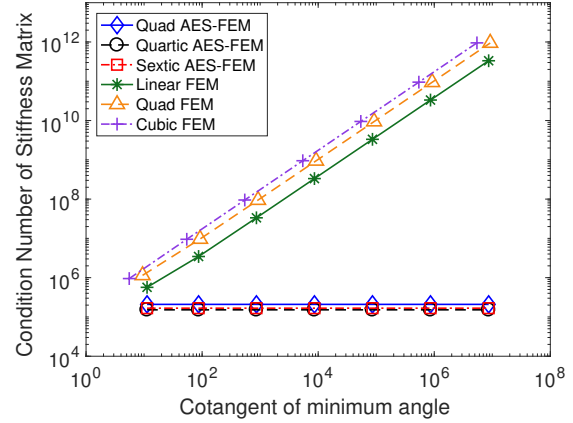


Figure 4: Comparison of condition numbers of AES-FEM and FEM with respect to min-angles.

In addition, the basis functions must be compatible with the test functions with respect to the bilinear form a in (15), so that the bilinear form does not vanish and does not blow up.

Under the quasiuniformity and stability conditions, we can also bound the relative condition number of the linear system (18). For second-order BVPs, $\|\mathbf{A}\| = \|\mathbf{M}\| \mathcal{O}(h^{-2})$, where h denotes some characteristic edge length, and hence

$$\kappa(\mathbf{A}) = \|\mathbf{A}\| \|\mathbf{A}^{-1}\| \leq \|\mathbf{M}\| \|\mathbf{A}^{-1}\| \mathcal{O}(h^{-2}) = \mathcal{O}(h^{-2}). \quad (58)$$

Similarly, $\kappa(\mathbf{M}^{-1}\mathbf{A}) = \mathcal{O}(h^{-2})$. This bound is well known for FDM and FEM. In general, $\kappa(\mathbf{A})$ determines the propagation of rounding errors and the convergence rate of iterative linear solvers without preconditioners. As long as the constant in front of h^{-2} is a small constant, the effect of $\kappa(\mathbf{A})$ on the overall accuracy and stability is negligible with a moderate h (i.e., a moderate-resolution mesh). Figure 3 shows $\kappa(\mathbf{A})$ of AES-FEM for the Poisson equation with Dirichlet boundary conditions in 2D for a series of meshes, and it is clear that $\kappa(\mathbf{A})$ is inversely proportional to h^2 .

However, $\kappa(\mathbf{A})$ has two implications. First, h in general should not be much smaller than the cubic root of the machine epsilon of the floating-point arithmetic, or the rounding errors may dominate truncation errors. This imposes a lower bound on h , and hence a high-order method may be needed to achieve a desired accuracy with low-precision floating-point arithmetic. Second, if the constant factor in front of h^{-2} is large, then the rounding errors may dominate, and it may become more difficult to construct effective preconditioners for the iterative solvers. Note that this constant factor may differ drastically for different methods. For FEM with linear elements, this constant is inversely proportional to the smallest angle of the elements in an asymptotic sense [15]. (Note that this differs from the *max-angle condition* of Babuška and Aziz [1], which is related to the errors in the gradient approximations with FEM basis functions instead of $\kappa(\mathbf{A})$.) In contrast, the condition number of AES-FEM (or GFDM) does not depend on element shapes. Figure 4 compares $\kappa(\mathbf{A})$ of AES-FEM to FEM for the Poisson equation with Dirichlet boundary conditions in 2D for a series of meshes with different minimum angles.

4.3 Convergence for Projection Problem

With Theorem 11, we can prove the convergence of a GWRM by establishing its local consistency. We first consider the projection problem (40), which is an important base case. Let \mathbf{f}_I be composed of $f(\mathbf{x}_i)$, and let $f_{I,i} = \Phi_i^T \mathbf{f}_I$. Furthermore, let the error vector be $\delta \mathbf{f} = \mathbf{f}_P - \mathbf{f}_I$ and $\delta f_i = f - f_{I,i}$. Then, we can apply Theorem 11 by replacing $a(\delta u_i, \psi_i)$ with $\langle \delta f_i, \psi_i \rangle_\Omega$.

Theorem 12. For the projection problem (40), suppose f is continuously differentiable to the p th order. Under the quasiuniformity condition (54), GWRM with degree- p Lagrange or GLP basis functions converge at the rate of at least $\mathcal{O}(h^{p+1})$ in the ℓ^2 -norm.

Proof. Under the differentiability assumption of f , from Lemma 2,

$$\|\delta f_i\|_\infty = \mathcal{O}(h^{p+1}). \quad (59)$$

Therefore, $|\langle \delta f_i, \psi_i \rangle_\Omega| \leq \int_\Omega |\psi_i| d\mathbf{x} \mathcal{O}(h^{p+1})$, and Theorem 11 implies $\mathcal{O}(h^{p+1})$ convergence rate in the ℓ^2 -norm. \square

The above proof holds for GFDM, AES-FEM, and FEM. In particular, for FEM, (59) is also applicable within each element. Note that the convergence rate in Theorem 12 is the worst case. In practice, the convergence rate may be higher for even-degree basis functions, as we will show in Section 5.

4.4 Convergence for Boundary Value Problems

We now use Theorem 11 to analyze the convergence of GWRM for solving boundary value problems with GLP basis functions, including GFDM and AES-FEM.

Lemma 13. For the second-order boundary value problem (2), suppose the exact solution u is continuously differentiable up to at least p th order. Then, in a GWRM with degree- p GLP basis functions, for each test function ψ_i ,

$$|a(\delta u_i, \psi_i)| \leq \rho_i \mathcal{O}(h^{p-1}), \quad (60)$$

where $\rho_i = \int_\Omega |\psi_i| d\mathbf{x}$.

Proof. Under the differentiability assumption of u , from Lemma 2,

$$\|\nabla^2(\delta u_i)\| = \mathcal{O}(h^{p-1}), \quad (61)$$

so is $|\mathcal{L}(\delta u_i)|$. Therefore, $|a(\delta u_i, \psi_i)| \leq \int_\Omega |\psi_i| d\mathbf{x} \mathcal{O}(h^{p-1})$. \square

We then obtain the following convergence result.

Theorem 14. For the second-order boundary value problem (2) with homogeneous boundary conditions, suppose f and the exact solution u are continuously differentiable to p th derivatives. Under the stability condition (56), the global errors in GFDM and AES-FEM with degree- p GLP basis functions converge at the rate of at least $\mathcal{O}(h^{p-1})$ in the ℓ^2 -norm, i.e., $\frac{1}{\sqrt{n}} \|\delta \mathbf{u}\| \leq \mathcal{O}(h^{p-1})$.

Proof. Note that $\max_i \{ \int_\Omega |\psi_i| d\mathbf{x} \} \leq \mathcal{O}(1) \|\mathbf{M}\|$ in both GFDM and AES-FEM. Hence, (60) in Lemma 13 implies the condition (57) in Theorem 11. \square

Theorem 14 implies that GFDM and AES-FEM converge with quadratic or higher-degree basis functions. If the gradient is needed, then $\nabla u \approx \nabla \Phi_i^T \mathbf{u}_h$ would converge locally for cubic or higher-degree basis functions. However, the convergence rate in Theorem 14 is the worst case, without assuming any symmetry of the mesh. More importantly, it does not take into account the orthogonality in the weighted residual formulation in AES-FEM, which may result in *superconvergence* depending on the order of the differential operator and the degree of the basis functions. We will consider these cases for AES-FEM in Section 5.

In terms of FEM, the worst-case convergence rate in Theorem 11 would be overly pessimistic, because it does not take into account the orthogonality property of the weighted residual formulation. For coercive PDEs with smooth solutions, it is well known that degree- p Galerkin FEM converges at $\mathcal{O}(h^{p+1})$ in the L^2 norm. This is typically proven using a global argument, namely the duality argument for symmetric bilinear forms. The $\mathcal{O}(h^{p-1})$ convergence rate in Theorem 14 is uncompetitive compared to that of FEM, because it is for general cases. In the following, we prove the superconvergence of GFDM and AES-FEM with even-degree basis functions using a local argument for the general bilinear form (35).

5 Superconvergence in AES-FEM

In this section, we analyze the superconvergence of GWRM, especially that of AES-FEM. Superconvergence enables higher accuracy at low cost, and hence it is of great theoretical and practical interest.

In general, there are three sources of superconvergence for a GWRM:

1. *antisymmetric stencils in differentiation*,
2. *antisymmetric local support in numerical integration*, and
3. *orthogonality in numerical integration*.

The first type is analogous to that of centered differences, and it is the only source of superconvergence for GFDM, which we analyze in Appendix D for completeness. The latter two types are applicable to GWRM with (weakly) differentiable test functions, including FEM and AES-FEM. The second type is due to the *symmetry* of the local support of a test function, or more precisely, the *antisymmetry* of the leading error term over the local support. This is similar to antisymmetric stencils in Appendix D, except that the test functions (and potentially also the basis functions) are piecewise over the local support. The analyses in [7] and [11], for example, consider this type of superconvergence. The third type is the primary source of superconvergence for FEM and AES-FEM. In a loose sense, it is analogous to the superconvergence of Gaussian quadrature rules, except that the GWRM depends on (approximate) orthogonality in the (generalized) weighted-residual formulation instead of the orthogonal polynomials. Unlike the first two types, the third type does not require symmetry in the mesh, so we focus on it here. This type of superconvergence cannot be analyzed by using Taylor series or the backward error analysis alone. In FEM, this analysis is done using the duality argument, which is global in nature and assumes the symmetry of the bilinear form. For AES-FEM, our analysis will be local in nature, without requiring symmetry of the bilinear form, through the aid of the discrete Green's functions.

5.1 Error Cancellation due to Orthogonality

We first show the following superconvergence of $\langle \delta u_{h,i}, \psi_i \rangle_\Omega$ in the ℓ^2 -norm, where $\delta u_{h,i} = u - u_{h,i}$.

Lemma 15. *For AES-FEM, $\langle \delta u_{h,i}, \psi_i \rangle_\Omega$ superconverges at the order of $\mathcal{O}(h^p)$ in the ℓ^2 -norm, i.e.,*

$$\|[\langle \delta u_{h,i}, \psi_i \rangle_\Omega]\| \leq \|\mathbf{M}\| \mathcal{O}(h^p). \quad (62)$$

In addition, if $\boldsymbol{\nu} = \mathbf{0}$, $\|[\langle \delta u_{h,i}, \psi_i \rangle_\Omega]\| \leq \|\mathbf{M}\| \mathcal{O}(h^{p+1})$.

Proof. Let \mathbf{u}_P be the AES-FEM projection of u with the test functions $\{\psi_i\}$ and basis functions $\{\Phi_i\}$ and let $u_{P,i} = \Phi_i^T \mathbf{u}_P$. Note that

$$\|[\langle \delta u_{h,i}, \psi_i \rangle_\Omega]\| \leq \|[\langle \delta u_{P,i}, \psi_i \rangle_\Omega]\| + \|[\langle u_{P,i} - u_{h,i}, \psi_i \rangle_\Omega]\|. \quad (63)$$

From Theorem 12,

$$\frac{1}{\sqrt{n}} \|[\langle \delta u_{P,i}, \psi_i \rangle_\Omega]\| \leq \|\mathbf{M}\| \mathcal{O}(h^{p+1}). \quad (64)$$

By definition, $\langle u_{P,i}, \psi_i \rangle = \langle u, \psi_i \rangle$. Therefore,

$$\begin{aligned} \langle u_{P,i} - u_{h,i}, \psi_i \rangle_\Omega &= \langle u - u_{h,i}, \psi_i \rangle_\Omega \\ &= \langle \delta u_{h,i}, \mathcal{L}\mathcal{G}_i \rangle_\Omega \\ &= \langle \mathcal{L}\delta u_{h,i}, \mathcal{G}_i \rangle_\Omega + \int_\Omega \delta u_{h,i} (2\boldsymbol{\nu} \cdot \nabla \mathcal{G}_i + \mathcal{G}_i \nabla \cdot \boldsymbol{\nu}) \, dx. \end{aligned}$$

From Theorem 14 and the fact that $\|\mathcal{G}_i\|_\infty = \mathcal{O}(h^2)$, we obtain

$$\langle \mathcal{L}\delta u_{h,i}, \mathcal{G}_i \rangle_\Omega \leq \|\mathbf{M}\| \mathcal{O}(h^{p+1}).$$

Therefore,

$$|\langle \delta u_{h,i}, \psi_i \rangle_{\Omega}| \leq \|\mathbf{M}\| \mathcal{O}(h^{p+1}) + \left| \int_{\Omega} \delta u_{h,i} (2\boldsymbol{\nu} \cdot \nabla \mathcal{G}_i + \mathcal{G}_i \nabla \cdot \boldsymbol{\nu}) \, d\mathbf{x} \right|,$$

where

$$\left| \int_{\Omega} \delta u_{h,i} (2\boldsymbol{\nu} \cdot \nabla \mathcal{G}_i + \mathcal{G}_i \nabla \cdot \boldsymbol{\nu}) \, d\mathbf{x} \right| \leq \|\mathbf{M}\| \mathcal{O}(h^p),$$

which vanishes if $\boldsymbol{\nu} = \mathbf{0}$. Therefore, $\frac{1}{\sqrt{n}} \|\langle u_{P,i} - u_{h,i}, \psi_i \rangle_{\Omega}\| \leq \|\mathbf{M}\| \mathcal{O}(h^p)$ in general and $\leq \|\mathbf{M}\| \mathcal{O}(h^{p+1})$ if $\boldsymbol{\nu} = \mathbf{0}$. Substituting it and (64) in (63) completes the proof. \square

The proof of Lemma 15 resembles the duality analysis of FEM for symmetric bilinear forms, in that the discrete Green's function serves the role of a dual problem. However, there are two important differences. First, the discrete Green's function is local, where the duality problem in FEM analysis is global. Second, Lemma 15 constructs a reference solution using projection, whereas the duality analysis in FEM uses interpolation to construct the reference solution. Third, Lemma 15 does not assume the symmetry of the bilinear form. Note that Lemma 15 does not depend on the GLP basis functions, so it is also directly applicable to linear FEM, where $p = 1$.

5.2 Superconvergence with Even-Degree AES-FEM

It is important to note that Lemma 15 does not imply that $\delta u_{h,i}$ converges at $\mathcal{O}(h^p)$ or $\mathcal{O}(h^{p+1})$, because the leading order term in $\delta u_{h,i}$ may still be $\mathcal{O}(h^{p-1})$, while its corresponding term in $\delta u_{h,i} \psi_i$ is antisymmetric within each element and hence cancels out in $\langle \delta u_{h,i}, \psi_i \rangle$. This is indeed the case for odd-degree AES-FEM, and it may also occur for odd-degree FEM with a skew-symmetric differential operator. However, such an antisymmetry is impossible with even-degree AES-FEM. We therefore have the following theorem.

Theorem 16. *For the second-order boundary value problem (2) with homogeneous boundary conditions, suppose f and the exact solution u are continuously differentiable to p th derivatives. Under the stability condition (56), AES-FEM with even-degree- p basis functions converges at the rate of $\mathcal{O}(h^p)$ in the ℓ^2 -norm.*

Proof. We prove by contradiction. If the leading term in $\delta u_{h,i}$ is $\mathcal{O}(h^{p-1})$, then

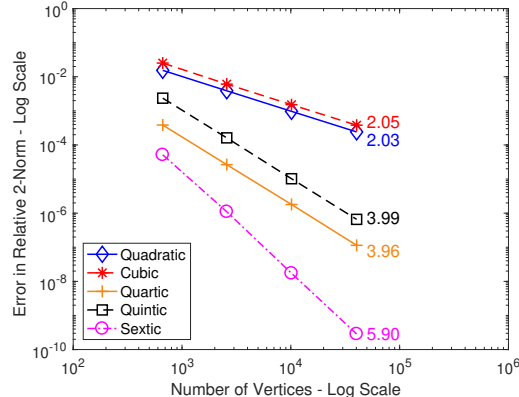
$$\delta u_{h,i} \psi_i = \delta u_{h,i}(\mathbf{x}_i) \Lambda_i + \mathbf{C} \bullet (\mathbf{x} - \mathbf{x}_i)^p \Lambda_i + \mathcal{O}(h^{p+1}),$$

where \mathbf{C} is a constant p th rank tensor. For even p , both $\delta u_{h,i}(\mathbf{x}_i) \Lambda_i$ and $\mathbf{C} \bullet (\mathbf{x} - \mathbf{x}_i)^p \Lambda_i$ are even functions about \mathbf{x}_i , and it is impossible for (62) to hold in Lemma 15. \square

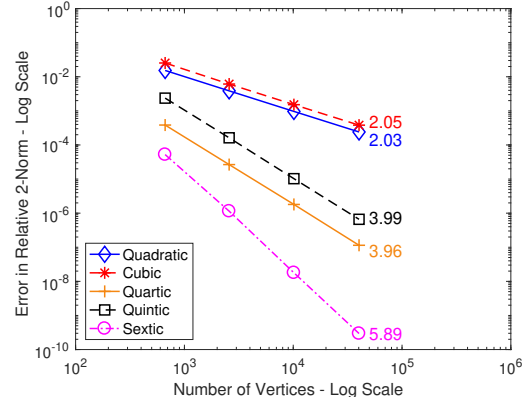
In the above proof, the evenness of the functions plays the essential role in translating the superconvergence of the numerical integration into the superconvergence of the solution. In FEM, this role is played by the coercivity of the discrete form of the PDE. However, the coercivity argument in FEM does not apply to AES-FEM because of the local nature of the GLP basis functions, so we cannot expect to achieve the $\mathcal{O}(h^{p+1})$ superconvergence of FEM in AES-FEM. The $\mathcal{O}(h^p)$ convergence rate in Theorem 16 is tight for even-degree AES-FEM, and the $\mathcal{O}(h^{p-1})$ rate in Theorem 14 is tight for odd-degree AES-FEM. In general, *we should match the parity of the order of the differential operator and the degree of the GLP basis functions*. As an illustration, we use AES-FEM with degrees 2–6 to solve the boundary-value equation

$$-\Delta u + \boldsymbol{\nu} \cdot \nabla u = f, \quad (65)$$

with unstructured meshes over $[-1, 1]^2$ with homogeneous boundary conditions, where $f = \sin \pi x \sin \pi y$. Figure 5(a) and (b) show the convergence results in the ℓ^2 -norm for $\boldsymbol{\nu} = [x, -y]$ and $\boldsymbol{\nu} = \mathbf{0}$, which are the convection-diffusion and Poisson equations, respectively. The convergence results confirm our theoretical analysis. In Part II, we will address how to preserve this superconvergence rate with more general boundary conditions over domains with curved boundary and corners.



(a) Convection-diffusion equation.



(b) Poisson equation.

Figure 5: The errors in the function values from AES-FEM for 2D convection-diffusion and Poisson equations. The number to the right of each curve indicates the average convergence rate.

5.3 Superconvergence of Gradients

The superconvergence of $u \approx \Phi_i^T \mathbf{u}_h$ leads to the superconvergence of $\nabla u \approx \nabla \Phi_i^T \mathbf{u}_h$, as stated by the following corollary.

Corollary 17. *Under the same conditions as in Theorem 16, for even-degree- p AES-FEM, $\nabla u \approx \nabla \Phi_i^T \mathbf{u}_h$ converges at the rate of at least $\mathcal{O}(h^{p-1})$ in the ℓ^2 -norm.*

This $\mathcal{O}(h^{p-1})$ convergence rate of the gradients is higher than the worst-case $\mathcal{O}(h^{p-2})$ in Section 4.4, so it is also a superconvergence phenomenon. Note that for FEM, the gradients superconverge at the same rate of the solution (i.e., $\mathcal{O}(h^{p+1})$) after a post-processing step using L^2 projection; see, e.g., [17, Section 15.4]. For AES-FEM, the gradients may also superconverge at the same rate as the solution (i.e., $\mathcal{O}(h^p)$ with even p), even without using projection for post-processing. In addition, the $\mathcal{O}(h^p)$ superconvergence rate of the gradient can also be achieved using a mixed formulation. We will defer the detailed descriptions and analyses of these techniques to Part III when we analyze AES-FEM for systems of partial differential equations.

6 Conclusions

In this paper, we introduced the framework of *generalized weighted residual methods (GWRM)*, which unifies FEM and (G)FDM. Based on this framework, we introduce a new class of high-order methods, namely *AES-FEM*, which is a hybrid of FEM and GFDM. We introduced a unified convergence analysis of GWRM with homogeneous boundary conditions. This analysis integrates, and generalizes, the components from functional and matrix analyses, most notably, the d -dimensional Taylor series, a discrete inf-sup condition, and a discrete Green's function. Our analysis establishes the worst-case convergence rates of FEM, GFDM, and AES-FEM for the projection problem as well as boundary value problems. In addition, we proved the superconvergence of GFDM with (nearly) uniform meshes and of AES-FEM for quasiuniform meshes.

The flexibility and generality of the GWRM framework have allowed us to combine the advantages of FEM and GFDM and overcome their respective disadvantages. In particular, AES-FEM enjoys simplified computation of second-order derivatives the FEM, while like GFDM, it is independent of element shapes. In addition, like GFDM on nearly uniform meshes, AES-FEM on quasiuniform meshes can achieve $\mathcal{O}(h^p)$ superconvergence rate for even-degree- p GLP basis functions for second-order BVPs, regardless of whether the bilinear form is symmetric. This is in contrast to FEM, which achieves $\mathcal{O}(h^{p+1})$ superconvergence rate for coercive BVPs with symmetric bilinear forms, regardless of whether p is even or odd. The lower convergence rate of AES-FEM is the cost for gaining independence of element shapes. However, the sparsity patterns of the stiffness matrix associated with degree- p AES-FEM are similar to those of degree- $(p-1)$ FEM, because the basis functions of the latter are piecewise. Hence, the primary additional cost of AES-FEM (and also of

GFDM to some extent) is the computations of the GLP basis functions on unstructured meshes. The main potential of AES-FEM, however, is to enable the possibility to develop more sophisticated hybrid GWRM methods that combine FEM and AES-FEM to achieve optimal accuracy, efficiency, and robustness, which we will explore in some future work.

In this part, we considered only homogeneous boundary conditions for simplicity. Although it is straightforward to treat other Dirichlet boundary conditions, we defer the general treatment of boundary conditions to Part II. A critical challenge in imposing boundary conditions is to match the convergence rate of the interior, especially along curved boundaries or at corners. We will address this challenge and will also report a comparative study in Part II. We will consider the solutions of systems of PDEs as well as the high-order recovery of the gradients in Part III.

Acknowledgements

Results were obtained using the high-performance LI-RED computing system at the Institute for Advanced Computational Science at Stony Brook University, which was obtained through the Empire State Development grant NYS #28451.

References

- [1] I. Babuška and A. K. Aziz. On the angle condition in the finite element method. *SIAM J. Numer. Anal.*, 13(2):214–226, 1976.
- [2] J. Benito, F. Ureña, and L. Gavete. Solving parabolic and hyperbolic equations by the generalized finite difference method. *J. Comput. Appl. Math.*, 209(2):208–233, 2007.
- [3] S. C. Brenner and R. Scott. *The Mathematical Theory of Finite Element Methods*, volume 15. Springer Science & Business Media, 2008.
- [4] R. Conley, T. J. Delaney, and X. Jiao. Overcoming element quality dependence of finite elements with adaptive extended stencil FEM (AES-FEM). *Int. J. Numer. Meth. Engng.*, 2016. doi:10.1002/nme.5246.
- [5] J. Douglas and T. Dupont. Superconvergence for Galerkin methods for the two point boundary problem via local projections. *Numerische Mathematik*, 21(3):270–278, 1973.
- [6] J. Douglas Jr, T. Dupont, and M. F. Wheeler. An L^∞ estimate and a superconvergence result for a Galerkin method for elliptic equations based on tensor products of piecewise polynomials. *RAIRO Anal. Numer.*, 8:61–66, 1974.
- [7] A. Ern and J.-L. Guermond. *Theory and Practice of Finite Elements*, volume 159. Springer Science & Business Media, 2013.
- [8] B. A. Finlayson. *The Method of Weighted Residuals and Variational Principles*. Academic Press, New York, 1973.
- [9] G. Fix and G. Strang. Fourier analysis of the finite element method in Ritz-Galerkin theory. *Studies in Applied mathematics*, 48(3):265–273, 1969.
- [10] J. Humphreys, T. J. Jarvis, and E. J. Evans. *Foundations of Applied Mathematics, Volume I: Mathematical Analysis*. SIAM, 2017.
- [11] X. Jiao. Quasicentroidal simplicial meshes for optimal variational methods. In *27th Annual Fall Workshop on Computational Geometry*, Stony Brook, NY, Nov. 2017.
- [12] X. Jiao and D. Wang. Reconstructing high-order surfaces for meshing. *Engineering with Computers*, 28(4):361–373, 2012.
- [13] T. Liszka and J. Orkisz. The finite difference method at arbitrary irregular grids and its application in applied mechanics. *Comput Struct*, 11(1-2):83–95, 1980.

- [14] N. Ray, D. Wang, X. Jiao, and J. Glimm. High-order numerical integration over discrete surfaces. *SIAM J. Numer. Anal.*, 50(6):3061–3083, 2012.
- [15] G. Strang and G. J. Fix. *An Analysis of the Finite Element Method*, volume 212. Prentice-Hall Englewood Cliffs, NJ, 1973.
- [16] J. C. Strikwerda. *Finite difference schemes and partial differential equations*. SIAM, 2004.
- [17] O. C. Zienkiewicz, R. L. Taylor, and J. Z. Zhu. *The Finite Element Method: Its Basis and Fundamentals*. Butterworth-Heinemann, 7th edition, 2013.

A Computation of GLP Basis Functions

Given a node \mathbf{x}_0 , let \mathbf{v} denote the local coordinate system centered at it. Let $\mathcal{P}_k^{(p)}(\mathbf{x})$ denote the set of all d -dimensional monomials of degree p and lower; for example, $\mathcal{P}_2^{(2)}(\mathbf{x}) = [1, x, y, x^2, xy, y^2]^T$. Let $\mathbf{D}_k^{(p)}$ be a diagonal matrix consisting of the fractional factorial part of the coefficients in the Taylor series corresponding to $\mathcal{P}_k^{(p)}$; for example, $\mathbf{D}_2^{(2)} = \text{diag}(1, 1, 1, 1/2, 1, 1/2)$. Let \mathbf{c} be a vector containing the partial derivative of f evaluated at \mathbf{x}_0 ; for example, $\mathbf{c}^T = [f, f_x, f_y, f_{xx}, f_{xy}, f_{yy}]|_{\mathbf{x}=\mathbf{x}_0}$. Then, we may write the truncated Taylor series of a smooth function f as

$$f(\mathbf{x}) \approx \mathbf{c}^T \mathbf{D}_k^{(p)} \mathcal{P}_k^{(p)}(\mathbf{x}). \quad (66)$$

Suppose there are n coefficients in \mathbf{c} , and the stencil about the point \mathbf{x}_0 contains m points, include the point \mathbf{x}_0 . To obtain the j th basis function ϕ_j , let $f(\mathbf{x}_i) = \delta_{ij}$, the Kronecker delta function. Therefore, we obtain an $m \times n$ least squares problem

$$\mathbf{V}\mathbf{c}_j \approx \mathbf{e}_j, \quad (67)$$

where \mathbf{e}_j denote the j th column of the $m \times m$ identity matrix, and \mathbf{V} is the generalized Vandermonde matrix. Eq. (67) may potentially be ill-conditioned and potentially rank deficient, even if $m \geq n$. We solve (67) by minimizing a weighted norm (or semi-norm)

$$\min_{\mathbf{c}} \|\mathbf{V}\mathbf{c}_j - \mathbf{e}_j\|_{\mathbf{W}} \equiv \min_{\mathbf{c}} \|\mathbf{W}(\mathbf{V}\mathbf{c}_j - \mathbf{e}_j)\|_2, \quad (68)$$

where \mathbf{W} is an $m \times m$ diagonal weighting matrix, and it is a constant for a given node. In general, heavier weights are assigned to nodes that are closer to \mathbf{x}_0 ; for example,

$$w_i = \left(\frac{\|\mathbf{v}_i\|}{h} + \epsilon \right)^{-p/2}, \quad (69)$$

where ϵ is a small number, such as $\epsilon = 0.01$, for avoiding division by zero.

The matrix \mathbf{WV} can be poorly scaled. We address this by right-multiplying a diagonal matrix \mathbf{S} , a procedure that is referred to as *matrix equilibration*. Let \mathbf{a}_j denote the j th column of an arbitrary matrix \mathbf{WV} . A typical choice for the i th entry of \mathbf{S} is either $1/\|\mathbf{a}_i\|_2$ or $1/\|\mathbf{a}_i\|_\infty$. After weighting and scaling, the least-squares problem becomes

$$\min_{\mathbf{d}} \|\tilde{\mathbf{V}}\mathbf{d} - \mathbf{W}\mathbf{e}_j\|_2, \quad \text{where } \tilde{\mathbf{V}} \equiv \mathbf{WV}\mathbf{S} \text{ and } \mathbf{d} \equiv \mathbf{S}^{-1}\mathbf{c}_j. \quad (70)$$

We solve the problem using the truncated QR factorization with column pivoting, where the pivoting scheme is customized to preserve low-degree terms. The solution of the least squares problem is $\mathbf{c}_j = \mathbf{S}\tilde{\mathbf{V}}^+\mathbf{W}\mathbf{e}_j$. The complete set of basis functions is then given by

$$\Phi = \left(\mathbf{S}\tilde{\mathbf{V}}^+\mathbf{W} \right)^T \mathbf{D}\mathcal{P}. \quad (71)$$

B WALF and CAES-FEM

Let Λ_i denote that hat function at node \mathbf{x}_i , and let $\Phi_C = \sum_{i=1}^n \Lambda_i \Phi_i$, which is composed of basis functions

$$\phi_{C,j} = \sum_{i=1}^n \Lambda_i \phi_{ij}. \quad (72)$$

Then, we obtain a C^0 continuous solution

$$u_{h,C} = \Phi_C^T \mathbf{u}_h = \sum_{i=1}^n \Lambda_i (\Phi_i^T \mathbf{u}_h) = \sum_{i=1}^n \Lambda_i u_{h,i}. \quad (73)$$

Effectively, $u_{h,C}$ blends the nodal approximations $u_{h,i}$ with the hat functions; its gradient is given by

$$\nabla u_{h,C} = \sum_{i=1}^n \Lambda_i \nabla \Phi_i^T \mathbf{u}_h + \sum_{i=1}^n (\nabla \Lambda_i) \Phi_i^T \mathbf{u}_h. \quad (74)$$

We refer to the above approximation as *Weighted Averaging of Least Squares* or *WALF*, and it was used in [12] in high-order surface reconstructions and in [14] for high-order surface integration. The approximation power of Φ_C inherits those of the GLP basis functions Φ_i .

Substituting (73) into (37) and (22), we then obtain the coefficient matrix and its corresponding mass matrix

$$\mathbf{A} = a(\Phi_C, \Psi_\circ^T)^T = [a(\phi_{C,j}, \psi_i)], \quad (75)$$

$$\mathbf{M} = \langle \Phi_C, \Psi_\circ^T \rangle_\Omega^T = [\langle \phi_{C,j}, \psi_i \rangle_\Omega]. \quad (76)$$

Then $\mathbf{A}\mathbf{u}_h = \mathbf{b}$ gives the algebraic equation for CAES-FEM. Since Λ_i is only weakly differentiable, one must use the bilinear form (12) instead of (15) to compute (75). More importantly, the exact computation of gradients in (74) depends on element shapes, so would the global accuracy of CAES-FEM if (74) is used. Note that $\nabla u_{h,C}$ is approximated by $\sum_{i=1}^n \Lambda_i \nabla \Phi_i^T \mathbf{u}_h$ in [14] for computing surface integrals. However, the exact computation of (74) is required to maintain CAES-FEM as a Petrov-Galerkin FEM, so CAES-FEM is dependent on element shapes.

C Equivalence of Inf-Sup and Discrete Inf-Sup Conditions

To see this, consider an FEM with global basis functions Φ and test functions Ψ , where Φ may or may not be the same as Ψ . Let $\phi = \Phi^T \mathbf{u}$, and $\psi = \Psi^T \mathbf{v}$. For a linear BVP problem with homogeneous boundary conditions,

$$a(\phi, \psi) = \mathbf{u}^T \mathbf{A}^T \mathbf{v} \quad (77)$$

Let \mathbf{M}_Φ and \mathbf{M}_Ψ denote the mass matrices associated with the solution and test spaces, respectively, i.e.,

$$\mathbf{M}_\Phi = \langle \Phi, \Phi^T \rangle_\Omega \quad \text{and} \quad \mathbf{M}_\Psi = \langle \Psi, \Psi^T \rangle_\Omega. \quad (78)$$

Both \mathbf{M}_Φ and \mathbf{M}_Ψ are symmetric and positive definite, and

$$\|\phi\|_{L^2} = \sqrt{\mathbf{u}^T \mathbf{M}_\Phi \mathbf{u}} \quad \text{and} \quad \|\psi\|_{L^2} = \sqrt{\mathbf{v}^T \mathbf{M}_\Psi \mathbf{v}}. \quad (79)$$

Hence,

$$\sqrt{\lambda_{\min}(\mathbf{M}_\Phi) \lambda_{\min}(\mathbf{M}_\Psi)} \leq \frac{\|\phi\|_{L^2} \|\psi\|_{L^2}}{\|\mathbf{u}\| \|\mathbf{v}\|} \leq \sqrt{\lambda_{\max}(\mathbf{M}_\Phi) \lambda_{\max}(\mathbf{M}_\Psi)},$$

and

$$\frac{\mathbf{u}^T \mathbf{A}^T \mathbf{v} / (\|\mathbf{u}\| \|\mathbf{v}\|)}{\sqrt{\lambda_{\max}(\mathbf{M}_\Phi) \lambda_{\max}(\mathbf{M}_\Psi)}} \leq \frac{a(\phi, \psi)}{\|\phi\|_\Phi \|\psi\|_\Psi} \leq \frac{\mathbf{u}^T \mathbf{A}^T \mathbf{v} / (\|\mathbf{u}\| \|\mathbf{v}\|)}{\sqrt{\lambda_{\min}(\mathbf{M}_\Phi) \lambda_{\min}(\mathbf{M}_\Psi)}}.$$

Assume the mesh is *quasiuniform*, so that the ratio between the largest and smallest elements is bounded by a constant [3, 7]. Let V_i denote the volume of the local support for ϕ_i . It can be shown that for FEM,

$$\kappa(\mathbf{M}_\Phi) \leq \kappa_\phi \frac{\sup_i V_i}{\inf_i V_i} = \Theta(1), \quad (80)$$

where κ_ϕ is the condition number of the element mass matrix over the “master element” in the parametric space. Similarly, $\kappa(\mathbf{M}_\Psi) = \Theta(1)$. Hence,

$$\lambda_{\max}(\mathbf{M}_\Phi) = \Theta(1)\lambda_{\min}(\mathbf{M}_\Phi) \quad \text{and} \quad \lambda_{\max}(\mathbf{M}_\Psi) = \Theta(1)\lambda_{\min}(\mathbf{M}_\Psi). \quad (81)$$

Then, the inf-sup condition (25) is equivalent to

$$\exists \alpha' > 0, \quad \frac{\inf_{\|\mathbf{u}\|=1} \sup_{\|\mathbf{v}\|=1} \mathbf{u}^T \mathbf{A}^T \mathbf{v}}{\sqrt{\lambda_{\max}(\mathbf{M}_\Phi) \lambda_{\max}(\mathbf{M}_\Psi)}} = \frac{\sigma_{\min}(\mathbf{A})}{\sqrt{\lambda_{\max}(\mathbf{M}_\Phi) \lambda_{\max}(\mathbf{M}_\Psi)}} \geq \alpha'. \quad (82)$$

The Cauchy-Schwarz inequality in functional analysis is

$$|\mathbf{u}^T \mathbf{M}^T \mathbf{v}| = \langle \phi, \psi \rangle_\Omega \leq \|\phi\|_{L^2} \|\psi\|_{L^2} \leq \sqrt{\lambda_{\max}(\mathbf{M}_\Phi) \lambda_{\max}(\mathbf{M}_\Psi)} \|\mathbf{u}\| \|\mathbf{v}\|,$$

where the bound is tight for some \mathbf{u} and \mathbf{v} , and its counterpart in matrix analysis is

$$|\mathbf{u}^T \mathbf{M}^T \mathbf{v}| \leq \sigma_{\max}(\mathbf{M}) \|\mathbf{u}\| \|\mathbf{v}\|,$$

where the bound is also tight for some \mathbf{u} and \mathbf{v} . Hence,

$$\sqrt{\lambda_{\max}(\mathbf{M}_\Phi) \lambda_{\max}(\mathbf{M}_\Psi)} = \Theta(1) \sigma_{\max}(\mathbf{M}), \quad (83)$$

for sufficiently fine meshes, and hence (25) is equivalent to (52).

D Error Cancellation in Numerical Differentiation

The superconvergence of GFDM depends on the *symmetry* of the stencil, or more precisely, the *antisymmetry* of the leading error term over the stencil. This is analogous to the error cancellation in centered differencing on uniform structured grids. For unstructured meshes in d -dimensions, we formalize this notion of antisymmetry as follows.

Definition 18. Given a k th-order differential operator \mathcal{L} , a *stencil* $\{\mathbf{x}_j \mid 1 \leq j \leq m\}$ for degree- p GLP basis functions $\{\phi_j\}$ is *nearly antisymmetric* about \mathbf{x}_0 if

$$\left\| \sum_{j=1}^m \mathcal{L}\phi_j(\mathbf{x}_0) (\mathbf{x}_j - \mathbf{x}_0)^{p+1} \right\| = \mathcal{O}(h^{p-k+2}). \quad (84)$$

In (84), $\mathcal{L}\phi_j(\mathbf{x}_0)$ corresponds to the coefficients in finite differences. In general, (near) antisymmetry can only occur if $p - k + 1$ is odd (i.e., p and k have the same parity), so that the weighted sum in (84) is an odd function about \mathbf{x}_0 . This is the reason of the name “antisymmetry” instead of “symmetry.” In addition, it can occur only if the stencil is well balanced about \mathbf{x}_0 , and conversely, it is impossible along (or near) boundaries, where the stencils are one-sided. GFDM superconverges with nearly antisymmetric stencils for boundary value problems.

Corollary 19. For the second-order boundary value problem (2), suppose the exact solution u is continuously differentiable to at least $(p+1)$ st order. In GFDM with even-degree- p GLP basis functions, if the stencil is nearly antisymmetric with respect to \mathcal{L} about \mathbf{x}_i , then

$$|\delta u_i(\mathbf{x}_i)| \leq \mathcal{O}(h^p). \quad (85)$$

If all the stencils are nearly antisymmetric, then the solution of the BVP converges at the rate of $\mathcal{O}(h^p)$ in the ℓ^2 -norm under the stability condition (56).

Proof. Let $u_{\mathbf{x}_i;p}$ denote the degree- p Taylor polynomial of the exact solution u about \mathbf{x}_i , i.e., the first-term in (27). Let $\mathbf{u}_{i,p}$ be the vector composed of $u_{\mathbf{x}_i;p}(\mathbf{x}_j)$. Then, for each point \mathbf{x}_j in the local stencil S , its corresponding entry in $\mathbf{u}_I - \mathbf{u}_{i,p}$ is given by

$$u(\mathbf{x}_j) - u_{\mathbf{x}_i;p}(\mathbf{x}_j) = \frac{1}{(p+1)!} \nabla^{p+1} u(\mathbf{x}_i) \bullet (\mathbf{x}_j - \mathbf{x}_i)^{p+1} + \mathcal{O}(h^p).$$

Assume $p \geq 2$. Then,

$$\mathcal{L}u(\mathbf{x}_i) = \mathcal{L}u_{\mathbf{x}_i;p}(\mathbf{x}_i) = \mathcal{L}\Phi_i^T(\mathbf{x}_i)\mathbf{u}_{i,p},$$

and

$$\begin{aligned} \mathcal{L}\delta u_i(\mathbf{x}_i) &= \mathcal{L}u(\mathbf{x}_i) - \mathcal{L}\Phi_i^T(\mathbf{x}_i)\mathbf{u}_I \\ &= \mathcal{L}\Phi_i^T(\mathbf{x}_i)(\mathbf{u}_{i,p} - \mathbf{u}_I) \end{aligned} \tag{86}$$

$$= -\frac{1}{(p+1)!} \nabla^{p+1} u(\mathbf{x}_i) \bullet \left(\sum_{j=1}^n \mathcal{L}\phi_{ij}(\mathbf{x}_i)(\mathbf{x}_j - \mathbf{x}_i)^{p+1} \right) + \mathcal{O}(h^p). \tag{87}$$

If the stencil is nearly antisymmetric, the leading term is also $\mathcal{O}(h^p)$. Hence, GFDM superconverges at $\mathcal{O}(h^p)$ due to Theorem 11. \square

Under the condition for Corollary 19, $\|\nabla\delta u_i(\mathbf{x}_i)\|_\infty$ converges at $\mathcal{O}(h^{p-1})$. We can adapt Corollary 19 to show that if a function f is continuously differentiable to $(p+1)$ st order and the stencils are nearly antisymmetric with respect to the identity map, then GFDM projection with even-degree- p GLP basis functions converges at the rate of $\mathcal{O}(h^{p+2})$ in the ℓ^2 -norm under the quasiuniformity condition (54). Of course, this superconvergence is only possible for points away from the boundary. The above analysis may be used to show the superconvergence of derivatives at some special points (such as the centroid) of an element. However, it does not apply to high-order AES-FEM (or FEM) in 2D or 3D, for which the derivatives are evaluated at high-degree quadrature points, instead of at nodes or centroids.